This is a postprint and has been peer-reviewed. The final published version of this manuscript is available online at the Journal of Marine and Petroleum Geology website. DOI: https://doi.org/10.1016/j.marpetgeo.2022.105629

The development of the eastern Orpheus rift basin, offshore eastern Canada: A case study of the interplay between rift-related faulting and salt deposition and flow

Bari R. Hanafi[1*], Martha O. Withjack[1], Michael A. Durcanin[1,2], Roy W. Schlische[1]

[1]Department of Earth and Planetary Sciences, Rutgers University, Piscataway, New Jersey, 08854, USA
[2]Murphy Exploration and Production Company, Houston, Texas 77024, USA
*Corresponding author email: brhanafi@eps.rutgers.edu

ABSTRACT

The salt-rich Orpheus rift basin, part of the eastern North American (ENAM) rift system, formed during the Late Triassic to Early Jurassic prior to opening of the Atlantic Ocean. Using a dense grid of 2D seismic-reflection lines, data from nearby wells, and information from adjacent ENAM rift basins, we have established a tectonostratigraphic framework, identified key structural elements, and reconstructed the deformation history for the eastern part of the basin. Our work shows that a series of E-striking, S-dipping faults with normal separation bound the basin on the north. Deformation within the basin is complex with forced folds above deep-seated intrabasin faults, detachment folds, detached thrust faults, and salt diapirs. The synrift evaporite sequence consists of an older massive salt unit that underlies a younger unit with two distinct interfingering facies. Facies A, consisting of salt and interbedded sedimentary rocks (likely shales), developed near the border-fault system and its relay ramps. Facies B, consisting of massive salt with few interbedded sedimentary rocks, developed toward the basin center. The youngest synrift unit accumulated exclusively within minibasins near the northern border-fault system. Based on location, this youngest synrift unit likely consists of coarse-grained and poorly sorted alluvial-fan or talus-slope deposits shed from the footwall. All synrift units are intruded by igneous sheets likely associated with the Central Atlantic Magmatic Province and, thus, are

mostly Late Triassic in age (or possibly older). The border-fault system profoundly affected deposition within the eastern Orpheus rift basin by providing pathways for clastic sediment input into the salt-rich basin. These depositional patterns subsequently influenced deformation associated with lateral salt flow during minibasin formation. In regions with interbedded salt, detachment folds and thrust faults developed, whereas salt walls and stocks developed in regions with more massive salt.

Keywords: *Orpheus rift basin; Eastern North American rift system; Rift-basin development; Synrift salt; Salt tectonics; Seismic interpretation.*

1. INTRODUCTION

The eastern North American (ENAM) rift system that formed during the breakup of Pangea extends from the southeastern United States to southeastern Canada. It has three geographic segments with distinct tectonic histories (Fig. 1a). Rifting was underway in all segments by Late Triassic time, but rifting ceased diachronously, first in the southern segment (latest Triassic/earliest Jurassic), then in the central segment (Early Jurassic), and finally in the northern segment (Early Cretaceous) (Withjack et al., 1998; Withjack and Schlische, 2005; Withjack et al., 2012).

Outcrop data (together with limited borehole and seismic-reflection data) from the exposed onshore rift basins have supplied important information about the stratigraphy, structure, and tectonic history of the ENAM rift system (e.g., Olsen et al., 1996; 2003; Schlische et al., 2003; Withjack et al., 2009; Withjack et al., 2013; Withjack et al., 2020). Critical questions, however, remain about the subsurface geology and timing of deformation for the ENAM rift system. The availability of high-quality, industry borehole and seismic-reflection data from several of the

offshore ENAM rift basins provide the opportunity to address these questions by better defining the subsurface stratigraphy and structure of the ENAM rift system and constraining the timing of deformation and, thus, the tectonic history of the ENAM margin during and after rifting.

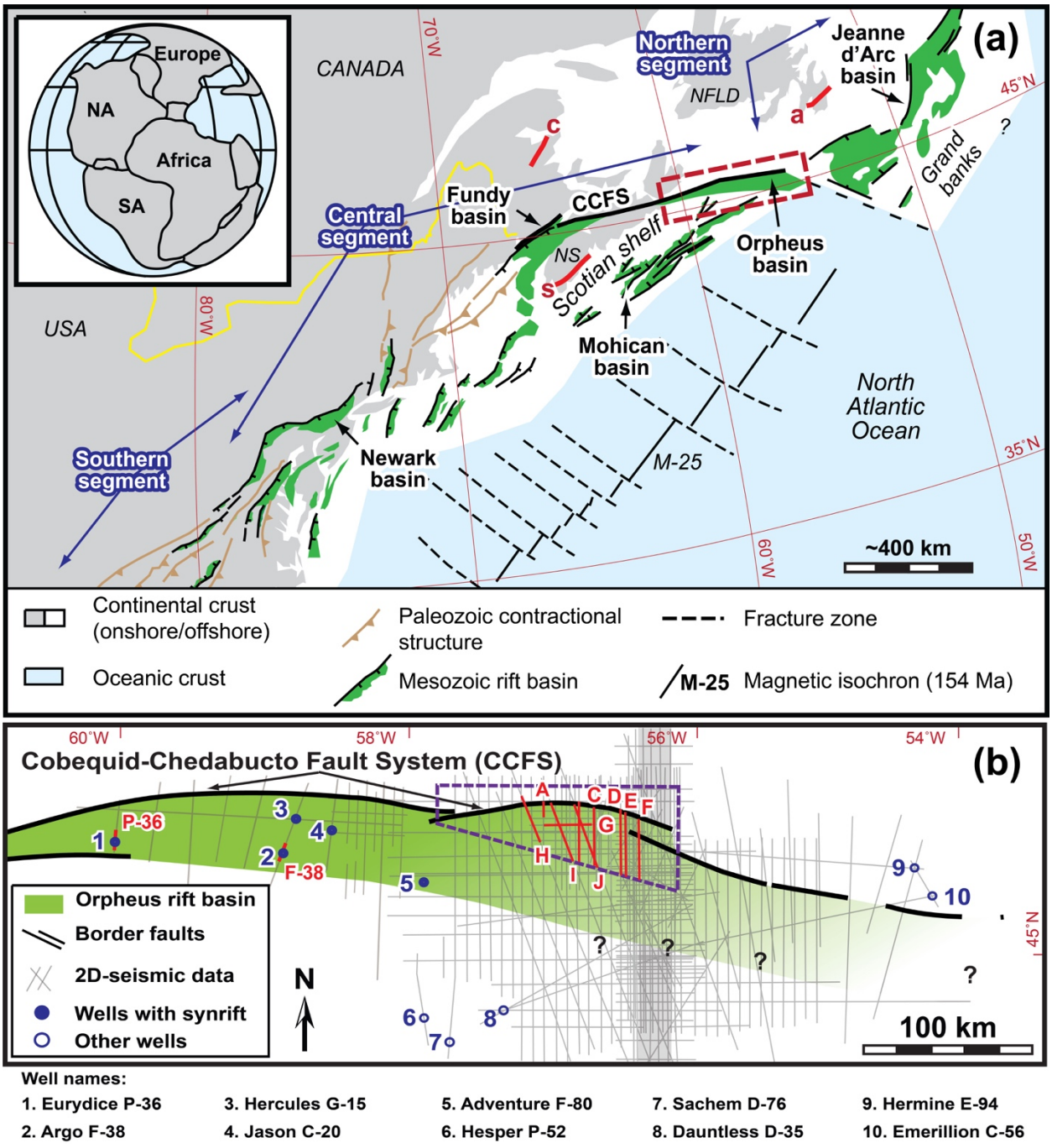

Figure 1. (a) *Regional map of eastern North America showing major Paleozoic contractional structures, Mesozoic rift basins, and tectonic features (modified from Withjack et al., 2012).*

Yellow line shows boundary between Canada and the United States of America. Dashed red box shows approximate location of area in Figure 1b. Inset map shows Pangean supercontinent during Late Triassic (after Olsen, 1997). NA: North America; NFLD: Newfoundland; NS: Nova Scotia; SA: South America. Thick solid black lines are Cobequid-Chedabucto fault system (CCFS). Red lines are select outcrops of intrusive rocks of the Central Atlantic Magmatic Province (CAMP) near study area, a: Avalon dike; c: Caraquet dike; s: Shelburne dike. ***(b)*** *Location map of Orpheus rift basin showing seismic and well data used in this study. Dashed polygon is focus area shown in Figures 4 and 13. Red, labeled lines are seismic profiles discussed in the paper. Stacking velocities from Lines I and J were used to determine interval velocities shown in Table 1.*

The Orpheus rift basin, located in offshore Nova Scotia and Newfoundland, Canada, is the northernmost rift basin in the central segment of the ENAM rift system (Fig. 1a). Previous studies, using primarily well data from the western Orpheus rift basin, have identified synrift clastic and evaporitic sedimentary rocks, including massive and interbedded salt (MacLean and Wade, 1993; Tanner and Brown, 2003). To complement these studies from the western Orpheus basin, we have used a dense-grid of high-quality 2D seismic-reflection lines (Fig. 1b) to establish a tectonostratigraphic framework, characterize the basement-involved and detached structures, determine the timing of deformation, and identify large-scale depositional patterns in the eastern Orpheus rift basin.

Specifically, this study addressed the following questions: 1) What is the basic geometry of the eastern Orpheus basin? 2) How does deformation vary temporally and spatially throughout the eastern Orpheus basin? 3) How do the synrift strata vary within the eastern Orpheus basin,

and how does this variability affect the mechanical stratigraphy and deformation within the basin? Answers to these questions will lead to a better understanding of the development of the Orpheus rift basin and other rift basins of the ENAM rift system as well as the complex interplay between rift-related faulting, salt deposition, and salt flow during and after rifting.

2. GEOLOGIC OVERVIEW OF THE ORPHEUS RIFT BASIN AND SURROUNDING REGION

Rifting in the central segment of the eastern North American (ENAM) rift system began by the Late Triassic and ended in the Early Jurassic when continental breakup occurred (e.g., Manspeizer, 1988; Manspeizer and Cousminer, 1988; Olsen, 1997; Withjack and Schlische, 2005; Olsen and Et-Touhami, 2008; Withjack et al., 2012). The Grand Banks region immediately to the north of the Orpheus rift basin is part of the northern segment of the ENAM rift system with rift onset by the Late Triassic but breakup occurring much later in the Cretaceous (Withjack and Schlische, 2005; Welsink and Tankard, 2012; Withjack et al., 2012).

In latest Triassic/earliest Jurassic time, a short-lived (< 1 my), but widespread, igneous event associated with the Central Atlantic Magmatic Province (CAMP) affected the entire ENAM rift system (Verati et al., 2007; Marzoli et al., 2011; Blackburn et al., 2013; Davies et al., 2017; Marzoli et al., 2019). The absolute age of CAMP is ~ 201 Ma based on isotopic dating of both intrusive and extrusive rocks (Verati et al., 2007; Marzoli et al., 2011; Blackburn et al., 2013; Davies et al., 2017; Marzoli et al., 2019). CAMP-related igneous activity included the intrusion of diabase sheets and dikes and the eruption of basalts. In the region surrounding the Orpheus basin (Fig. 1a), CAMP-related igneous rocks include the North Mountain Basalt in the Fundy rift basin (Dostal and Greenough, 1992; Olsen and Et-Touhami, 2008; Cirilli et al., 2009; Jourdan et

al., 2009) and the Shelburne (Pe-Piper et al., 1992; Dostal and Durning, 1998; Dunn et al., 1998), Caraquet (Pe-Piper et al., 1992; Dostal and Durning, 1998), and Avalon dikes (Pe-Piper et al., 1992). CAMP-related basalts are also present in nearby wells in the region between the Fundy and Orpheus rift basins (White et al., 2017), and CAMP-related basalts have been encountered in wells and seismically imaged in the Mohican rift basin on the Scotian Shelf (e.g., Weston et al., 2012; Deptuck and Altheim, 2018) and in the Jeanne d'Arc rift basin of the Grand Banks region (Pe-Piper et al., 1992). In addition to CAMP, a younger postrift igneous event affected the region in Early Cretaceous time (Pe-Piper and Piper, 2004; Bowman et al., 2012).

After rifting and breakup, the region underwent thermal subsidence with intermittent, local faulting, uplift, and erosion, allowing accumulation of a thick postrift sequence consisting of mainly marine clastic and carbonate sedimentary rocks in a broad depression known as the Scotian basin (Wade and MacLean, 1990; MacLean and Wade, 1992; Wade et al., 1995; Weston et al., 2012). A breakup unconformity (BU), a major erosional surface that marks the rift/drift transition, separates the synrift strata from the overlying postrift strata on the Scotian Shelf (Wade and MacLean, 1990; MacLean and Wade, 1992, 1993; Wade et al., 1995; Weston et al., 2012; Deptuck and Altheim, 2018).

The timing of continental breakup in the region remains uncertain. Synrift rocks of Early Jurassic age (Sinemurian), mainly consisting of fluvial and shallow-water lacustrine sedimentary strata, are exposed in the adjacent ENAM Fundy rift basin (e.g., Olsen, 1997; Withjack et al., 2012; Sues and Olsen, 2015). Therefore, rifting continued into the Early Jurassic in the region. The age of the oldest postrift strata in the Scotian basin, however, is poorly constrained. Researchers initially assigned an Early Jurassic age (i.e., late Sinemurian-early Pliensbachian) for the oldest postrift strata in the Scotian basin (Barss et al., 1979; Wade and MacLean, 1990).

Recent biostratigraphic studies (Weston et al., 2012; Ainsworth et al., 2016), however, were unable to confirm this Early Jurassic age. Well analysis from the Offshore Energy Technical Research Association (OETR) suggests that the oldest drilled postrift strata in the Orpheus region is late Middle Jurassic (i.e., Bathonian) (see Chapter 4 of OETR, 2014). However, seismic data from the Scotian Shelf suggest that Jurassic strata progressively onlap onto the breakup unconformity (e.g., Deptuck and Altheim, 2018), indicating that postrift rocks of Early Jurassic age may have accumulated in the deeper parts of the Scotian basin near the site of breakup. Information from the conjugate margin of northwest Morocco suggests that the oldest postrift rocks are Sinemurian/Pliensbachian in age (Medina, 1995; Hafid, 2000), indicating that the cessation of rifting, continental breakup, and the onset of drifting occurred in Early Jurassic time (Withjack et al., 2012).

Information about the synrift rocks within the Orpheus rift basin is limited. Fluvial clastic sedimentary rocks of Late Triassic age crop out near the western end of the Orpheus rift basin (Tanner and Brown, 1999). Five wells in the western part of the basin reached synrift rocks. Of these, only the Eurydice P-36 and Argo F-38 wells penetrated a significant part of the synrift section; the other three wells (i.e., Adventure F-80, Hercules G-15, and Jason C-20 wells) drilled only the uppermost part (MacLean and Wade, 1992, 1993). In the Argo F-38 and Eurydice P-36 wells, salt of the Argo Formation overlies the Eurydice Formation (MacLean and Wade, 1992; Wade et al., 1995; Tanner and Brown, 2003; MacRae and Rankin, 2018) (Fig. 2). In these wells, the relatively undeformed Argo Formation consists of a lower massive salt unit and an upper unit

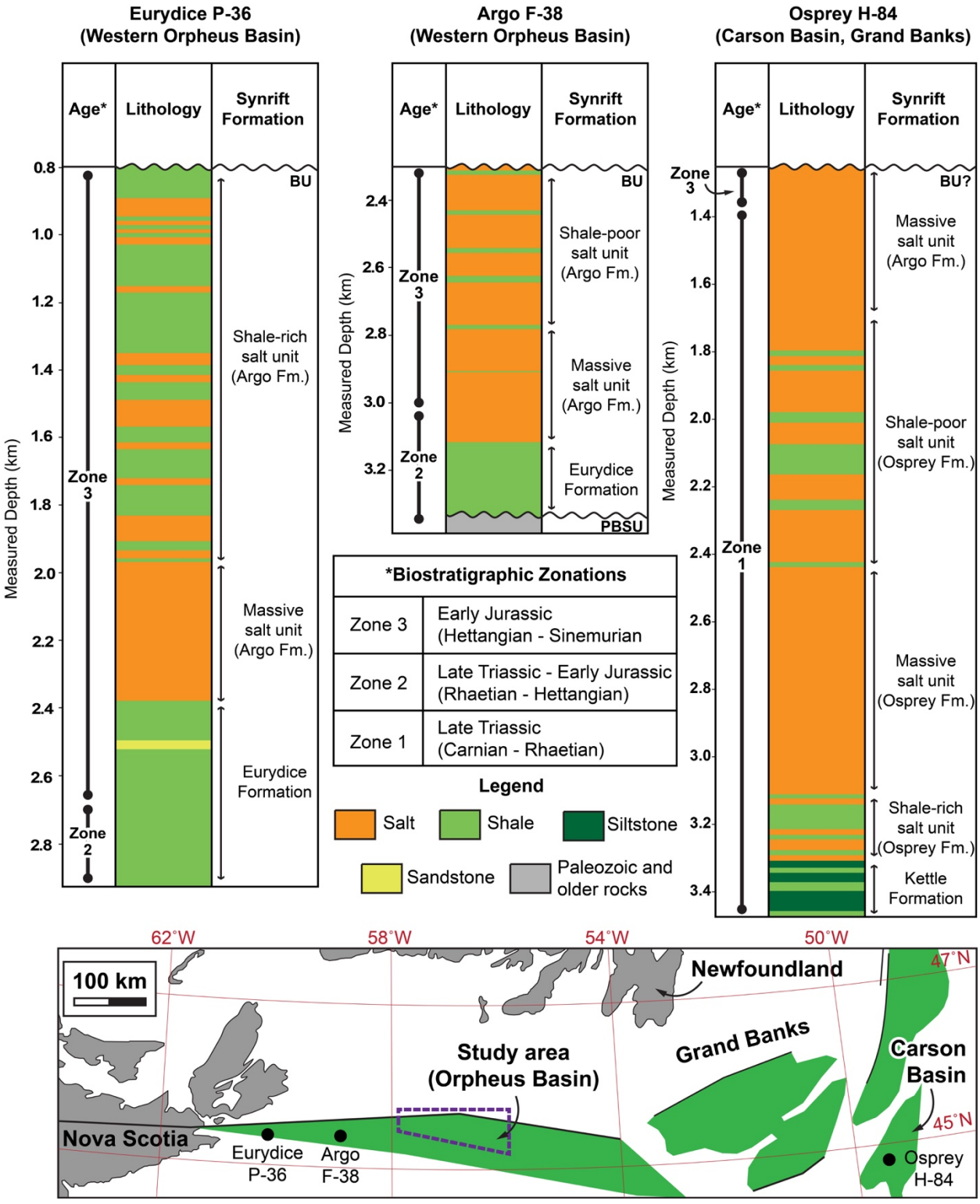

Figure 2. *Synrift lithologies from Eurydice P-36 (left) and Argo F-38 (middle) wells of the western Orpheus basin and Osprey H-84 (right) well of the Carson basin in the Grand Banks,*

showing the temporal and lateral variability of the synrift salt surrounding the study area. In all wells, clastic sedimentary rocks (i.e., the Eurydice and Kettle formations in the western Orpheus and Carson basins, respectively) underlie synrift salt that is Late Triassic-Early Jurassic in age. In the western Orpheus rift basin, the age of the synrift salt is mostly Early Jurassic consisting of lower massive salt and upper interbedded salt of the Argo Formation. The composition of the upper Argo Formation varies in both wells with more interbedded salt-shale in the Eurydice P-36 well and less interbedded salt-shale in the Argo F-38 well. The older synrift salt of Late Triassic age (i.e., Osprey Formation) in the Carson basin consists of massive salt and interbedded salt-shale units. Note that the study area is located between the Eurydice P-36 and Argo F-38 wells in the western Orpheus basin and the Osprey H-84 well in the Carson basin. Ages are based on biostratigraphic zonation by Barss et al. (1979). BU: Breakup unconformity; PBSU: Prerift/base synrift unconformity. Adapted from Holser et al. (1988) and MacLean and Wade (1993).

of interbedded salt and shale (Fig. 3). The amount of shale varies within the upper unit, ranging from shale-rich (shale-to-salt ratio of ~3:1) in the Eurydice P-36 well to relatively shale-poor (shale-to-salt ratio of ~1:10) in the Argo F-38 well (Fig. 2). The palynological age of the Argo Formation in these wells is Early Jurassic (Hettangian-Sinemurian) (Bujak and Williams, 1977; Barss et al., 1979; MacRae and Rankin, 2018). The continental red sandstones and shales of the underlying Eurydice Formation are dated as latest Triassic to earliest Jurassic (i.e., Rhaetian-Hettangian) (Bujak and Williams, 1977; Barss et al., 1979; MacRae and Rankin, 2018). Seismic-reflection data indicate that an estimated 2 km of older synrift rocks underlie the drilled section in the Eurydice P-36 well (Wade and MacLean, 1990; Tanner and Brown, 2003).

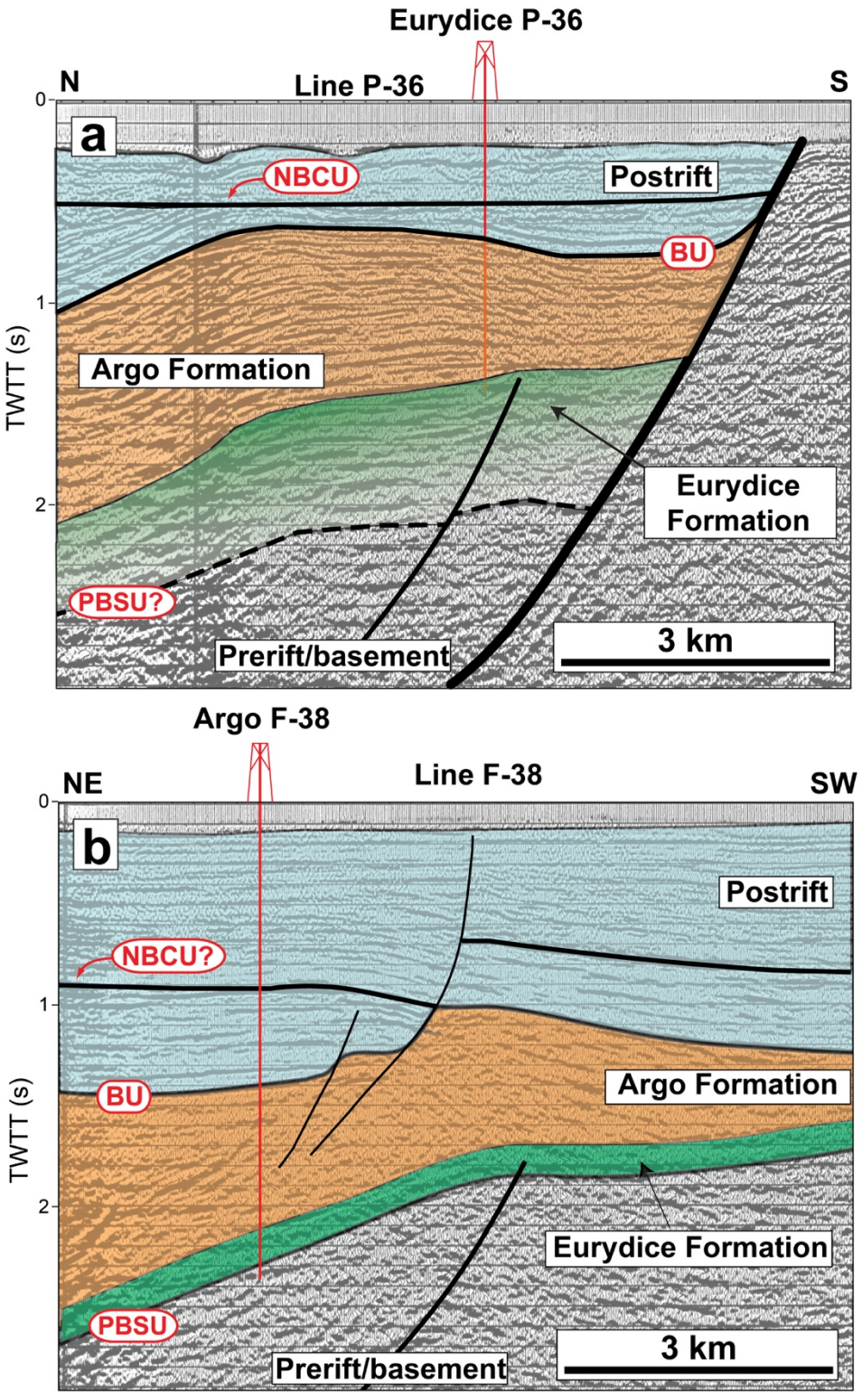

Figure 3. *Seismic interpretation of Lines P-36 and F-38 (see Fig. 1 for location). The Eurydice P-36 and Argo F-38 wells penetrated the synrift section in the western Orpheus rift basin. BU:*

breakup unconformity; NBCU: near-base Cretaceous unconformity; PBSU: Prerift/base synrift unconformity. Seismic lines are displayed 1:1 assuming a velocity of 4.5 km/s. Well-seismic correlations are from MacLean and Wade (1993).

No wells have penetrated the synrift section in the eastern Orpheus rift basin, but data from the surrounding ENAM rift basins and the conjugate margin of Morocco provide additional information about the possible ages and lithologies of the fill within the eastern part of the basin. Synrift rocks from the Scotian and Grand Banks regions, directly south and north of the eastern Orpheus rift basin (Figs. 1a, 2), respectively, include red sandstones and shales of Late Triassic age which underlie and/or interfinger with synrift salt of Late Triassic to Early Jurassic age (Tankard et al., 1989; Wade and MacLean, 1990; MacLean and Wade, 1992; Welsink and Tankard, 2012; Weston et al., 2012; Deptuck and Altheim, 2018). Similarly, synrift strata on the conjugate margin of Morocco consist of redbeds and synrift salt deposited during the Late Triassic and the Late Triassic-Early Jurassic, respectively (Hafid, 2000; Hafid et al., 2006; Tari and Jabour, 2013; Saura et al., 2014; Martin-Martin et al., 2017). In the Scotian and Grand Banks regions, some authors have subdivided the synrift salt into a lower unit of Late Triassic age called the Osprey Formation (Barss et al., 1979; Jansa et al., 1980; Holser et al., 1988; Manspeizer, 1988) and an upper unit of Late Triassic to Early Jurassic age called the Argo Formation (Holser et al., 1988; Sinclair, 1995; Sinclair et al., 1999) (e.g., Osprey H-84 well, Fig. 2). Others, however, refer to the entire salt package from the Scotian Shelf and Grand Banks regions as the Argo Formation (e.g., Sinclair, 1993; Kendell et al., 2012; Weston et al., 2012; Deptuck and Kendell, 2020). In this study, we refer to the synrift salt in the Orpheus rift basin, regardless of its age, as the Argo Formation.

3. SEISMIC-REFLECTION AND WELL DATA

This study uses more than 13,500 km of time-migrated, digital, 2D seismic-reflection profiles that cover >30,000 km^2 of offshore Nova Scotia and Newfoundland, Canada (Fig. 1b). These industry lines, acquired in the 1980s, 1990s, and 2000s, were processed using standard methods such as data resampling, bad-trace editing, deconvolution, velocity analysis, and the Kirchhoff pre-stack time migration (Yilmaz, 1987). In 2006, the Geological Survey of Canada reprocessed some key seismic profiles (acquired in 1984-1985), suppressing multiples and improving seismic imaging. The western part of the Orpheus rift basin has relatively low-quality seismic-reflection profiles (acquired in the 1980s) with line spacing of 15-20 km, whereas the eastern part of the basin has high-quality data (acquired mostly from 1998 to 2002) with line spacing of 2-5 km. The 2D seismic-reflection data have a sampling interval of 2-4 milliseconds and a record length of 8-12 seconds two-way travel time (TWTT).

To date the seismic horizons in the postrift section, we used biostratigraphic data from seven wells in the region (i.e., Argo F-38, Eurydice P-36 wells, Emerillon C-56, Hermine E-94, Sachem D-76, Hesper P-52, and Dauntless D-35 wells) (Barss et al., 1979; Ascoli, 1988; MacLean and Wade, 1993; Weston et al., 2012) (Fig. 1). The sonic-log and check-shot velocity data in these wells permit well-to-seismic correlation using synthetic seismograms (MacLean and Wade, 1993). Using the check-shot velocity data from the Eurydice P-36 and Argo F-38 wells and the interval velocities from three seismic lines in the study area, we estimated that the synrift section in the study area has an average seismic velocity of ~4.5 km/s (Table 1), similar to the velocity of rock salt (e.g., Willis et al., 2006; Zong et al., 2017). We used this value to display the seismic lines with approximately no vertical exaggeration at the level of the synrift section.

Table 1. *Interval velocities of postrift and synrift packages in the Orpheus rift basin based on check-shot velocities from two wells and interval velocities from three seismic-reflection profiles. See Figure 1b for well and seismic line locations and text for descriptions of postrift and synrift packages.*

Seismic Package	Check-shot Interval Velocity (km/s)		Seismic Interval Velocity (km/s)			Average Interval Velocity (km/s)
	Eurydice P-36	Argo F-38	Line H	Line I	Line J	
Postrift	2.8	3.0	2.4	2.6	2.5	2.6
Synrift	4.0	4.3	4.7	4.4	4.7	4.4

4. SEISMIC OBSERVATIONS AND INTERPRETATIONS

4.1. Deep-seated structures in the eastern Orpheus rift basin

The Cobequid-Chedabucto border-fault system (CCFS) forms the northern boundary of the eastern Orpheus rift basin and consists of several E-striking, right-stepping fault segments (Fig. 4). Two large, overlapping fault segments produce a 30-km-long relay ramp (i.e., a monoclinal fold that connects the footwall region to deeper parts of the hanging-wall basin) (Peacock and Sanderson, 1991; Schlische et al., 2002; Withjack et al., 2002). The border-fault segments dip to the south, have normal separation (e.g., Fig. 5), and locally have more than 5.5 km of offset (assuming a velocity of 4.5 km/s) (Fig. 4). Based on the kinematic linkage of the border-fault system of the Orpheus rift basin with that of the well-studied Fundy rift basin to the west (Fig. 1a), the border faults of the Orpheus rift basin likely had both normal and left-lateral components of slip during rifting that began by the Late Triassic and continued into the Early Jurassic (Withjack et al., 2009). Numerous deep-seated intrabasin faults with normal separation also

developed during rifting in the Orpheus rift basin (Fig. 4). In the study area, these intrabasin faults dip mainly toward the south and have offsets that range from hundreds of meters to several kilometers (assuming a velocity of 4.5 km/s).

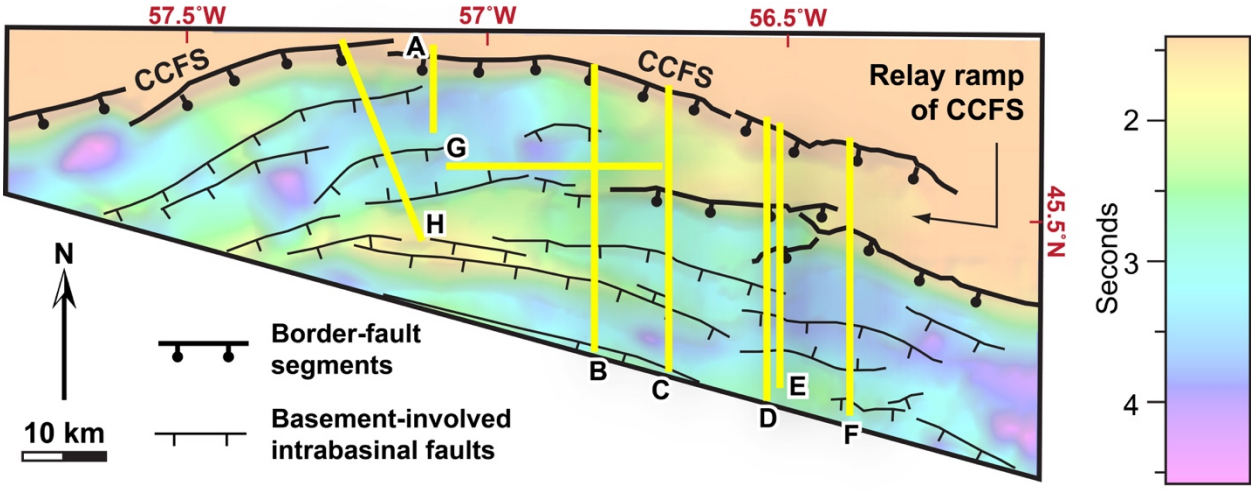

Figure 4. *Time-structure map of base of synrift salt south of the border-fault system and top of basement north of the border-fault system, showing basement architecture of eastern Orpheus rift basin (see Fig. 1 for location). Overlapping segments of border-fault system produced relay ramps. Color bar shows two-way travel time in seconds.*

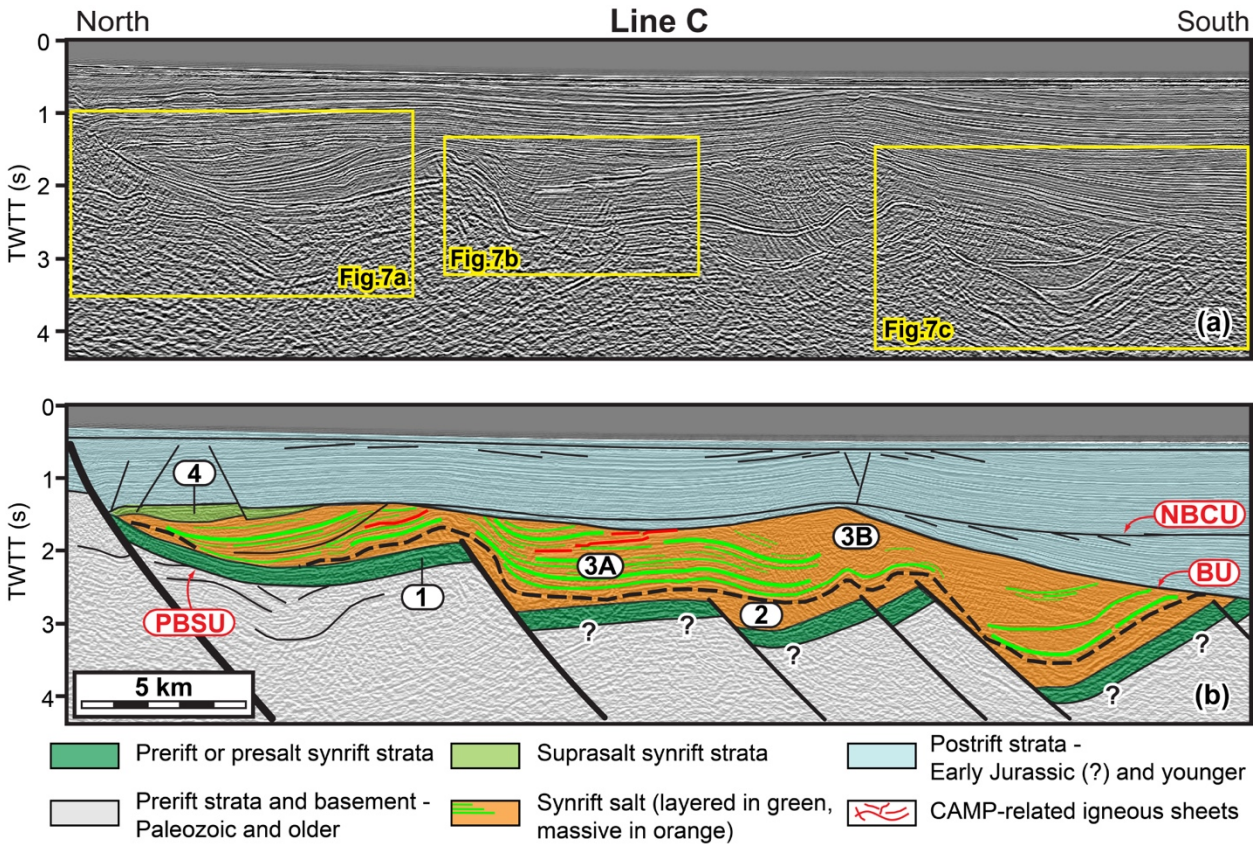

Figure 5. *Uninterpreted (**a**) and interpreted (**b**) versions of Line C (see Figs. 1b and 4 for location). The deepest tectonostratigraphic package (grey) includes prerift strata and basement. The oldest unconformity (the prerift/base synrift unconformity, PBSU) truncates folded prerift strata. The shallowest package (blue) is postrift strata. It is above the breakup unconformity (BU) and encompasses the near-base Cretaceous unconformity (NBCU). The middle package has four distinct seismic units: Unit 1 (synrift strata or prerift strata below salt, dark green), Unit 2 (lower massive synrift salt, orange), Unit 3 (upper synrift salt, orange with green lines), and Unit 4 (synrift strata above or adjacent to synrift salt, light green). Unit 3 has two facies. Facies 3A has numerous internal reflections (green lines), whereas Facies 3B is mostly transparent with few internal reflections. Thick solid black lines are segments of the border-fault system; thinner solid black lines are intrabasin faults. Black dashed line is approximate boundary between Units 2 and 3. Red lines are high-amplitude reflections interpreted as igneous*

sheets associated with CAMP, the Central Atlantic Magmatic Province. TWTT: Two-way travel time. Yellow boxes in Figure 5a show locations of seismic sections enlarged in Figure 7. Seismic line is displayed 1:1 assuming a velocity of 4.5 km/s.

4.2. Description and interpretation of major unconformities

We have identified three key unconformities in the study area (Fig. 6). 1) The deepest, oldest unconformity, imaged directly south of the border-fault system, separates truncated folded reflections from overlying, more gently folded reflections (Figs. 5, 7a). Based on previous studies in the region (e.g., Pascucci et al., 1999), the folded reflections beneath the unconformity are likely the deformed prerift Carboniferous strata above the prerift salt of the Windsor Formation. The age of the gently folded unit directly above the unconformity is uncertain. Thus, the unconformity might separate prerift and synrift strata. Alternatively, it might be an unconformity within the prerift section (Gibling et al., 2008). Based on this uncertainty, we label this unconformity the prerift/base synrift unconformity (PBSU; Fig. 6). 2) The second major unconformity separates truncated, tilted and folded reflections from overlying, gently to moderately tilted reflections (Figs. 5, 7b-c). Well data indicate that, in the southern part of the study area, the S-dipping reflections directly above the unconformity are associated with Jurassic postrift rocks. Thus, this unconformity is likely the breakup unconformity (BU; Fig. 6) recognized by others in the region (Wade and MacLean, 1990; MacLean and Wade, 1992, 1993; Wade et al., 1995; Deptuck and Altheim, 2018) and marking the transition from rifting to drifting. 3) The third unconformity is present throughout the study area (Fig. 5). Data from the Hermine E-94 and Emerillion C-56 wells indicate that, north of the border-fault system, the unconformity separates deformed Paleozoic prerift strata and basement from overlying,

relatively undeformed postrift strata of Early Cretaceous age (Wade and MacLean, 1990; MacLean and Wade, 1993; Pascucci et al., 1999). South of the border-fault system, the unconformity and breakup unconformity merge. Seismic correlation with the Dauntless D-35 well indicates that, in the southernmost part of the study area, the unconformity separates truncated, gently to moderately S-dipping, postrift strata of Late Jurassic age from overlying, relatively flat-lying, postrift strata of Early Cretaceous age (Fig. 5). Thus, we interpret this surface as the near-base Cretaceous unconformity (NBCU; Fig. 6), a major unconformity identified by Weston et al. (2012) based on biostratigraphic data from the Scotian basin. The NBCU in the study area corresponds to the widespread Avalon unconformity described by Wade and MacLean (1990) and MacLean and Wade (1992, 1993).

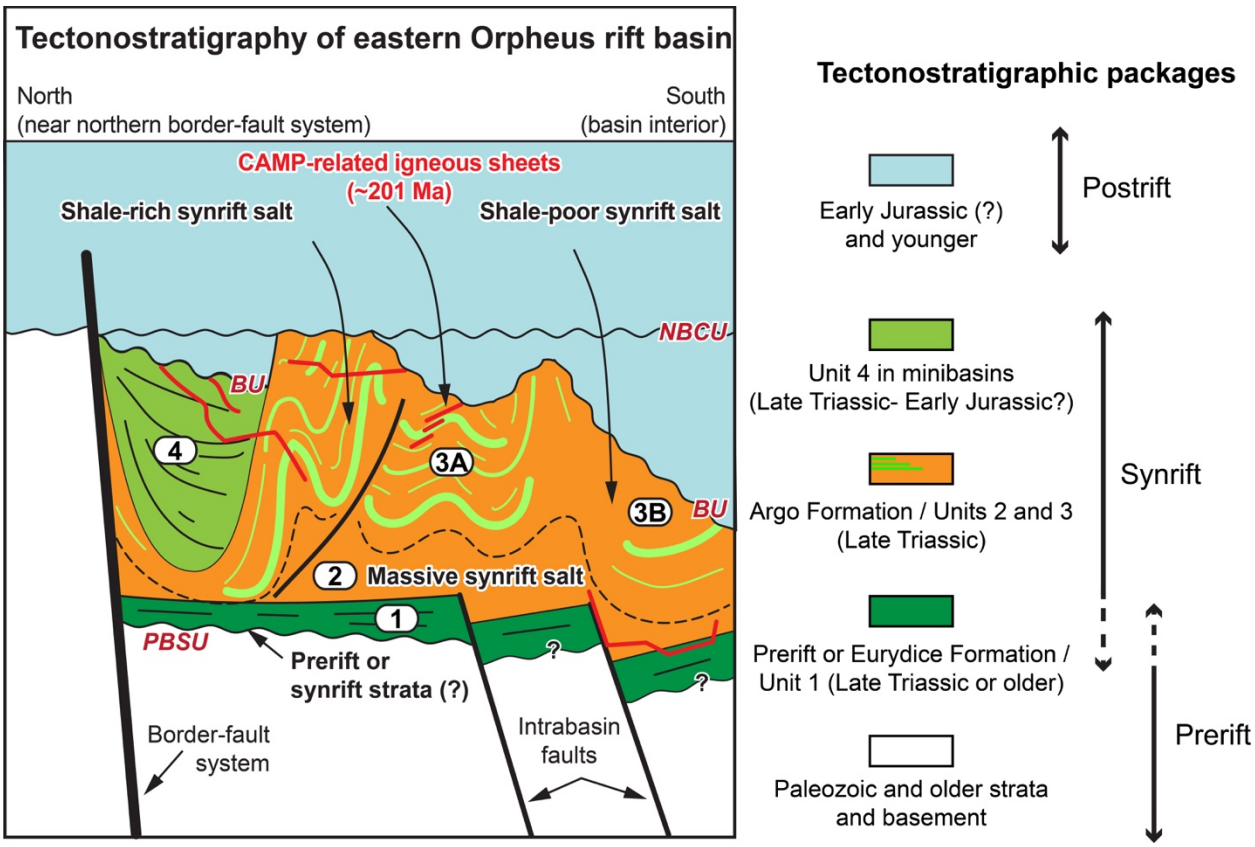

Figure 6. *Vertically exaggerated (~2.5x), schematic cross section showing proposed tectonostratigraphy of the eastern Orpheus rift basin. The synrift Argo Formation varies*

temporally with the massive salt of Unit 2 beneath the interbedded salt of Unit 3 and laterally with the shale-rich Facies 3A near the border-fault system and the shale-poor Facies 3B far from the border-fault system. CAMP-related igneous sheets are present within the eastern Orpheus rift basin, intruding all synrift units. Dashed black line indicates approximate boundary between Units 2 and 3. CAMP: Central Atlantic Magmatic Province. BU: Breakup unconformity; NBCU: Near-base Cretaceous unconformity; PBSU: Prerift/base synrift unconformity.

4.3. Description and interpretation of prerift and postrift packages

Three tectonostratigraphic packages are present in the eastern Orpheus rift basin (Figs. 5, 6). The oldest package is the prerift package. As discussed previously, north of the border-fault system, the prerift package consists of crystalline basement that underlies deformed Carboniferous strata (e.g., Pascucci et al., 1999; Gibling et al., 2008) as, for example, encountered in the Hermine E-94 and Emerillon C-56 wells (Wade and MacLean, 1990; MacLean and Wade, 1993). To the south, the prerift package is only imaged directly south of the border-fault system (e.g., northern part of Line C in Fig. 5) where, as discussed previously, it includes the folded Paleozoic strata imaged beneath the prerift/base synrift unconformity (PBSU) and possibly the unit directly above the unconformity.

The youngest tectonostratigraphic package is the postrift package. The lower part of the postrift package is only present in the southern parts of the study area between the breakup unconformity (BU) and the near-base Cretaceous unconformity (NBCU) (Fig. 5). It includes carbonate and clastic sedimentary rocks of Early (?) to Late Jurassic age (MacLean and Wade, 1992; Weston et al., 2012; Ainsworth et al., 2016). The upper part of the postrift package

unconformably overlies the lower postrift package in the southern parts of the study area, the merged BU and NBCU directly south of the border-fault system, and the footwall of the border-fault system in the northern part of the study area (Fig. 5). It consists mostly of gently folded to relatively flat-lying strata that are parallel-to-subparallel to the underlying NBCU, and includes carbonate and clastic sedimentary rocks of Early Cretaceous and younger age (MacLean and Wade, 1992; Weston et al., 2012; Ainsworth et al., 2016).

4.4. Description and interpretation of synrift package

The middle tectonostratigraphic package, the focus of this study, lies between the prerift and postrift packages and represents the synrift section of the eastern Orpheus rift basin (Fig. 6). As mentioned previously, the prerift/base synrift unconformity (PBSU) is at or near the base of the synrift package, whereas the breakup unconformity (BU) and the near-base Cretaceous unconformity (NBCU) define the top of the synrift package in the south and north, respectively (Figs. 7c-d). The basement-involved faults of the Cobequid-Chedabucto border-fault system (CCFS) form the northern boundary of the synrift package (Fig. 5). The thickness of the synrift package varies considerably in the study area, ranging from less than 1 km near the border-fault system to locally more than 5.5 km (assuming velocity of 4.5 km/s; Figs. 5, 8, 9).

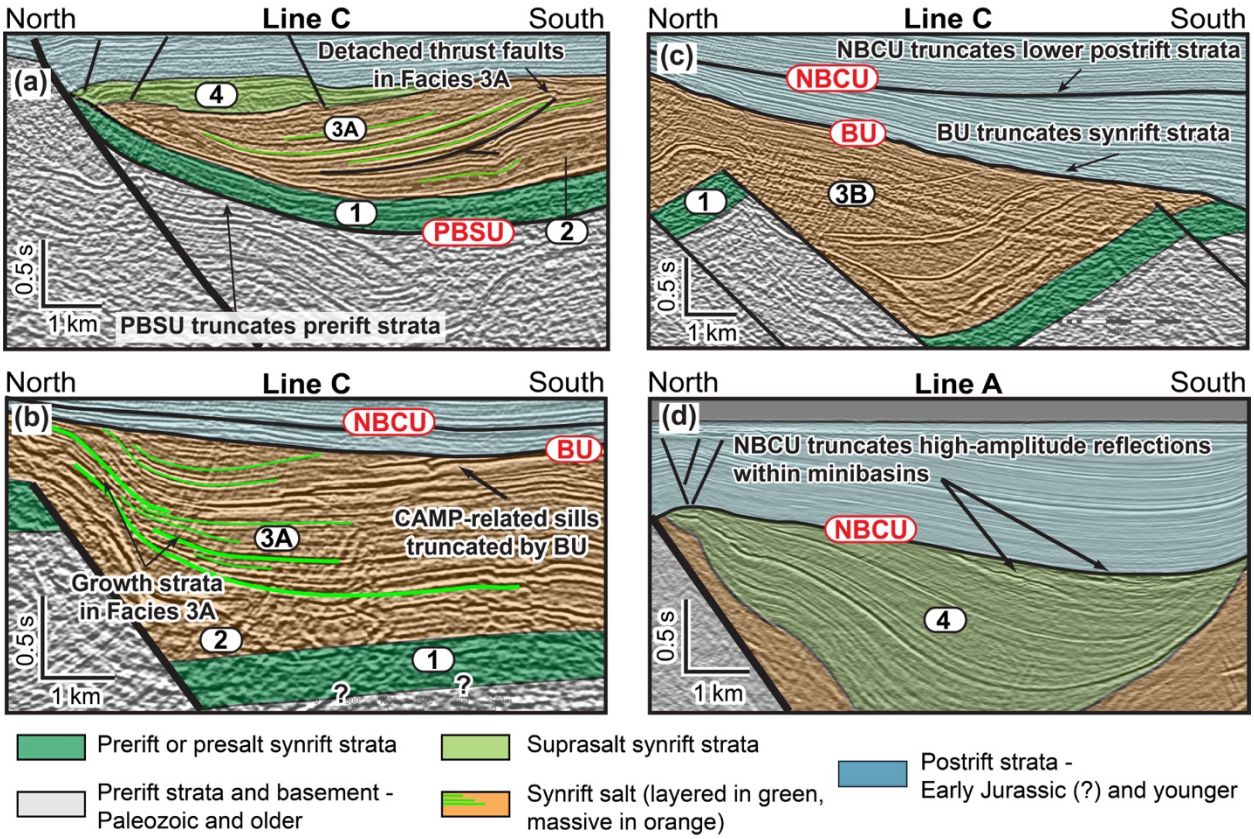

Figure 7*. Seismic lines showing detailed structural and stratigraphic features of prerift, synrift, and postrift sections in the eastern Orpheus rift basin. See caption of Figure 5 for description of Units 1-4. Thick solid black lines are segments of the border-fault system; thinner solid black lines are intrabasin faults.* ***(a)*** *Northern part of Line C (Fig. 5) showing truncation of folded prerift strata by prerift/base synrift unconformity (PBSU) and presence of detached thrust fault within Facies 3A.* ***(b)*** *Middle part of Line C (Fig. 5) showing forced-folded strata of Facies 3A that thin toward footwall of fault. Thickness changes are associated with growth and/or tectonic thinning.* ***(c)*** *Southern part of Line C (Fig. 5) showing breakup (BU) and near-base Cretaceous unconformities (NBCU) that truncate synrift and lower postrift strata, respectively.* ***(d)*** *Line A (see Fig. 1b for location) showing synrift strata above and/or adjacent to salt within minibasin and truncation of high-amplitude reflections interpreted as CAMP-related intrusives in*

minibasin by NBCU (near base Cretaceous unconformity). CAMP: Central Atlantic Magmatic Province. Seismic lines are displayed 1:1 assuming a velocity of 4.5 km/s.

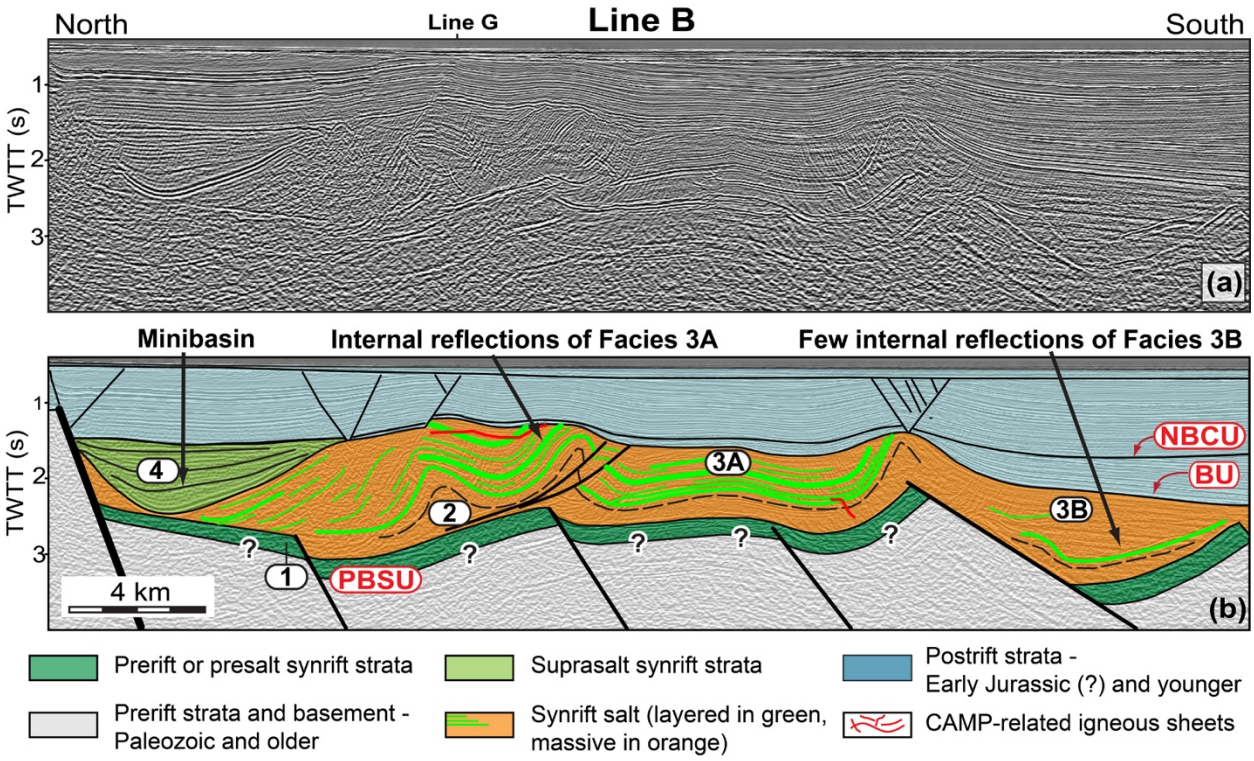

Figure 8. *Uninterpreted* ***(a)*** *and interpreted* ***(b)*** *versions of Line B (see Fig. 1b for location). See caption of Figure 5 for description of Units 1-4. Note that Line B shows predominantly folded strata of Facies 3A. Thick solid black lines are segments of the border-fault system; thinner solid black lines are intrabasin faults. Black dashed line is approximate boundary between Units 2 and 3. PBSU: Prerift/base synrift unconformity; BU: Breakup unconformity; NBCU: Near-base Cretaceous unconformity; PBSU: Prerift/base synrift unconformity. CAMP: Central Atlantic Magmatic Province. TWTT: Two-way travel time. Seismic line is displayed 1:1 assuming a velocity of 4.5 km/s.*

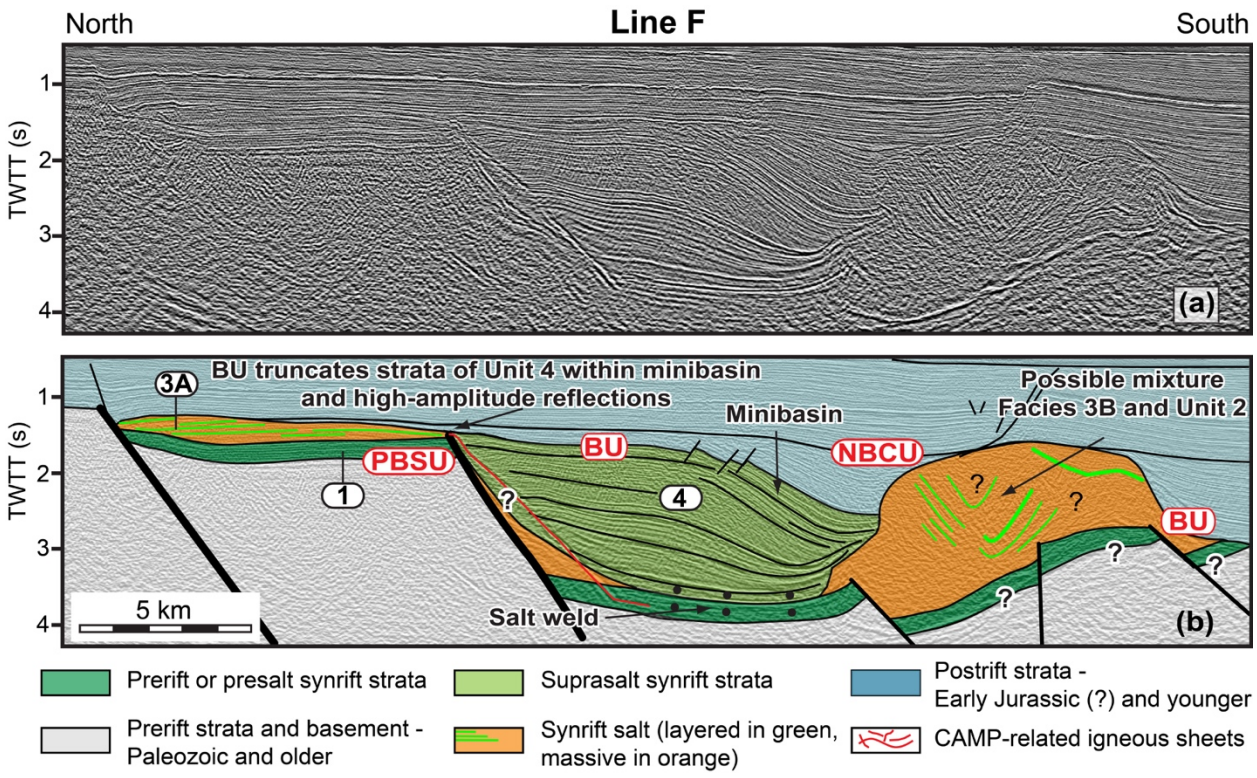

Figure 9. *Uninterpreted (**a**) and interpreted (**b**) versions of Line F (see Fig. 1b for location). See caption of Figure 5 for description of Units 1-4. The minibasin and salt wall developed synchronously. Note the salt weld at the base and the turtle structure within the minibasin. Thick solid black lines are segments of the border-fault system; thinner solid black lines are intrabasin faults. PBSU: Prerift/base synrift unconformity; BU: Breakup unconformity; NBCU: Near-base Cretaceous unconformity; CAMP: Central Atlantic Magmatic Province. TWTT: Two-way travel time. Seismic line is displayed 1:1 assuming a velocity of 4.5 km/s.*

We have subdivided the synrift package into four separate units with distinctive characteristics. No wells have penetrated these units in the study area, and the combination of intense deformation within the synrift package and widely spaced, poor quality seismic data from the western Orpheus rift basin prevents a direct seismic correlation with available well data from the western part of the Orpheus rift basin. We can infer, however, the lithology of these units

based on their seismic characteristics, their mechanical behaviors, and geologic information from the ENAM rift basins that surround the eastern Orpheus rift basin.

4.4.1. Synrift (?) Unit 1

Unit 1 directly overlies the folded prerift strata beneath the prerift/base synrift unconformity (PBSU) (Fig. 5). Its maximum thickness is ~0.4 s TWTT (~0.9 km), and it consists of subparallel reflections that are gently folded and offset by deep-seated intrabasin faults with normal separation. Unit 1, with its deep stratigraphic location and relatively brittle behavior, may be part of the Eurydice Formation, the oldest synrift formation in the region composed of clastic sedimentary rocks (Wade and MacLean, 1990; MacLean and Wade, 1992, 1993; Tanner and Brown, 2003) (Fig. 6). Alternatively, Unit 1, lacking clear rift-related growth geometries, may be part of the prerift package (Gibling et al., 2008) (Fig. 6).

4.4.2.Synrift Units 2 and 3

Unit 2 overlies Unit 1, lacks internal seismic reflections, and has significant thickness variations ranging from less than 0.1 s TWTT (~0.2 km) to ~1.5 s TWTT (~3.4 km) (Figs. 5, 8). For example, on Line C (Fig. 5), Unit 2 thins northward, becoming thin or absent near the border-fault system. Unit 2 also thickens within the cores of anticlines and thins beneath synclines (Fig. 8). In some parts of the basin, Unit 2 appears to mix with overlying Unit 3 forming tall masses (Fig. 9). Unit 2 commonly serves as a major detachment level within the synrift package, decoupling the deep and shallow deformation (Fig. 8). The characteristics of Unit 2 indicate a highly ductile behavior.

Unit 3 overlies Unit 2. Multiple seismic lines in the study area show a systematic change of Unit 3 in both the dip (N-S) and strike (E-W) directions relative to the border-fault system. For example, on Lines C, B, and D (Figs. 5, 8, 10), Unit 3 has numerous internal reflections in the north near the border-fault system and becomes more seismically transparent with fewer internal reflections in the south farther from the border-fault system. Similarly, on Line G (Fig. 11), the number of coherent internal reflections gradually decreases and the distance between these reflections increases toward the west moving down the relay ramp between the offset segments of the border-fault system (Fig. 4). Thus, Unit 3 has two end-member seismic facies (i.e., 3A and 3B). Facies 3A consists of numerous coherent and parallel-to-subparallel reflections, whereas Facies 3B is acoustically more transparent with fewer internal reflections (e.g., Fig. 5). These two facies have different deformational styles. Shortening-related structures such as detached folds and thrust faults are common in Facies 3A (Figs. 7a, 8), whereas Facies 3B, where deformed, forms large, tall bodies and exhibits highly ductile behavior (Fig. 9). Some of the transparency of Facies 3B is likely caused by intense deformation and the resultant lack of seismic coherency as discussed by Rowan et al. (2019). However, the transition from Facies 3A to Facies 3B occurs adjacent to zones of intense deformation (e.g., Line D, Fig. 10; Line G, Fig. 11), indicating that some of the transparency of Facies B is caused by an actual reduction of internal reflections, not only a lack of seismic coherency.

We interpret Units 2 and 3, with their highly ductile behavior and their stratigraphic position above Unit 1, as evaporite sequences within the Argo Formation (Fig. 6). The parallel-to-subparallel geometry of the reflections within Unit 3 suggest that the evaporite sequences were deposited in a broad, subsiding basin with most deformation occurring after deposition. Unit 2, lacking internal reflections, likely consists of massive salt, whereas Unit 3, with internal

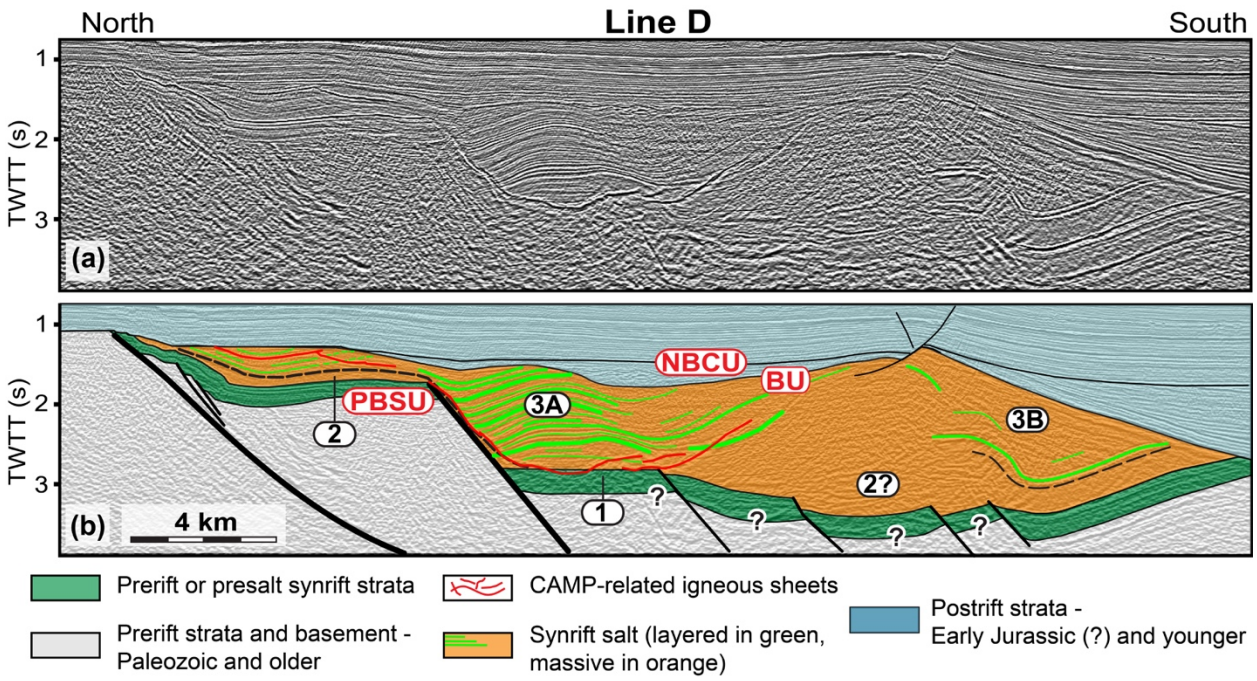

Figure 10. *Uninterpreted* ***(a)*** *and interpreted* ***(b)*** *versions of Line D (see Fig. 1b for location). See caption of Figure 5 for description of Units 1-4. Facies 3A with numerous internal reflections occurs near the border-fault system, whereas Facies 3B with few internal reflections occurs far from border-fault system. Thick solid black lines are segments of the border-fault system; thinner solid black lines are intrabasin faults. Black dashed line is approximate boundary between Units 2 and 3. PBSU: Prerift/base synrift unconformity; BU: Breakup unconformity; NBCU: Near-base Cretaceous unconformity; CAMP: Central Atlantic Magmatic Province; TWTT: Two-way travel time. Seismic line is displayed 1:1 assuming a velocity of 4.5 km/s.*

reflections, consists of salt with variable amounts of interbedded sedimentary layers (i.e., it is a layered evaporite sequence). Interbedded sedimentary layers in other salt basins include other evaporites (i.e., gypsum, anhydrite), carbonates, shales, siltstones, or igneous rocks (Van Gent et al., 2011; Jackson et al., 2015; Rowan et al., 2019). Well data from the western Orpheus rift

basin and the surrounding ENAM rift basins indicate that salt of the Argo Formation is interbedded mainly with shale (Holser et al., 1988; Wade and MacLean, 1990; MacLean and Wade, 1992, 1993; Weston et al., 2012) (Fig. 2). Therefore, we propose that Facies 3A and 3B of Unit 3 are shale-rich and shale-poor salt facies, respectively, of the Argo Formation (Fig. 6). Thus, the thick synrift package in the eastern Orpheus rift basin, with the exception of thin Eurydice Formation (?) at its base, is composed primarily of massive and interbedded rock salt of the Argo Formation.

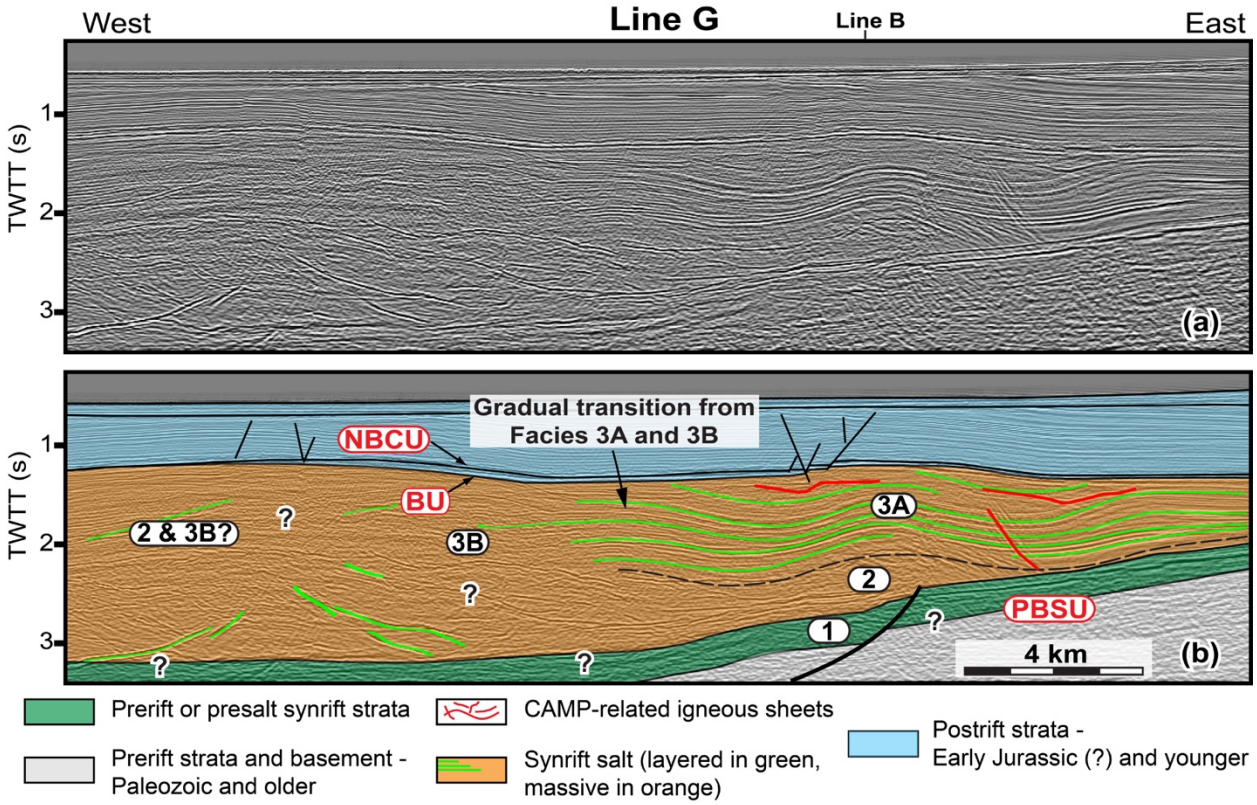

Figure 11. *Uninterpreted* ***(a)*** *and interpreted* ***(b)*** *versions of Line G (see Fig. 1b for location). See caption of Figure 5 for description of Units 1-4. The number of internal reflections and the distance between individual reflections within Unit 3 changes from east to west down the relay ramp of the border-fault system, reflecting the gradual transition from Facies 3A in the east to Facies 3B in the west. Solid black lines are intrabasin faults. BU: Breakup unconformity;*

NBCU: Near-base Cretaceous unconformity; PBSU: Prerift/base synrift unconformity. CAMP: Central Atlantic Magmatic Province; TWTT: Two-way travel time. Dashed black line indicates approximate boundary between Units 2 and 3. Seismic line is displayed 1:1 assuming a velocity of 4.5 km/s.

4.4.3. Synrift Unit 4

Unit 4 is the synrift component of fill within asymmetric synclines in the hanging-wall of the border-fault system (Figs. 7d, 9). The vertical thickness of Unit 4 can reach up to 2.5 s TWTT (~5.6 km). Reflections within Unit 4 either converge or diverge toward and/or onlap onto adjacent salt bodies composed of Units 2 and 3 (Fig. 9), indicating that Unit 4 was deposited during salt flow. This also suggests that sedimentary loading associated with the deposition of Unit 4 promoted lateral salt flow from beneath the synclines to the adjacent growing salt structures. Thus, these synclines are similar to the salt-withdrawal minibasins (Hudec et al., 2009; Goteti et al., 2012; Rowan, 2019) commonly observed in other salt provinces (e.g., Diegel et al., 1995; Callot et al., 2014; Saura et al., 2014; Martin-Martin et al., 2017; Teixell et al., 2017). Although both Unit 4 and Facies 3A of Unit 3 have numerous internal reflections and have similar seismic appearances, they differ fundamentally in that the reflections within Unit 4 truncate against the edges of growing salt bodies, whereas those within Facies 3A become incorporated into growing salt bodies.

No wells have penetrated the minibasins in the eastern Orpheus rift basin, making it difficult to interpret the lithology of the minibasin fill of Unit 4. Because the minibasins in our study area developed exclusively near the northern border-fault system, Unit 4 may consist, at least in part, of coarse-grained and poorly sorted, alluvial-fan deposits as commonly observed adjacent to the

border faults of other rift basins (e.g., Gawthorpe et al., 1990; Leeder and Jackson, 1993; Gupta et al., 1999; Allen and Heller, 2012; Ford et al., 2013) or rock-fall deposits associated with nearby fault talus, similar to that observed in the adjacent Fundy rift basin (Olsen and Schlische, 1990; Tanner and Hubert, 1991; Withjack et al., 2009; Withjack et al., 2010).

4.5. Detached structures in the eastern Orpheus rift basin

Detached structures are ubiquitous throughout the study area, reflecting the presence of highly ductile strata of the Argo Formations within the synrift package. Detached structures include forced folds, detachment folds, detached faults with normal and reverse separation, massive salt walls and stocks, and salt-withdrawal minibasins (Fig. 12c-h).

Forced folds are a type of fault-propagation fold that forms where the upward transition from faulting to folding is abrupt, signifying the presence of a highly ductile layer at depth (Jackson and Vendeville, 1994; Withjack and Callaway, 2000). In the eastern Orpheus rift basin, the presence of massive salt near the base of the synrift section (i.e., Unit 2) promoted the formation of forced folds above segments of the border-fault system and the intrabasin faults. For example, on Line C (Figs. 5, 7b), a forced fold developed above a segment of the upward-propagating border-fault system. The folded strata associated with Facies 3A dip and thicken toward the south away from the border-fault system. These thickness changes are likely associated with tectonic thinning and/or growth related to deposition of Facies 3A during the forced folding and faulting. Forced folds also developed above the intrabasin faults in the south (Fig. 5). There, the folded strata of Facies 3A exhibit no significant thickness changes, indicating that the forced folding and intrabasin faulting occurred after the deposition of Facies 3A.

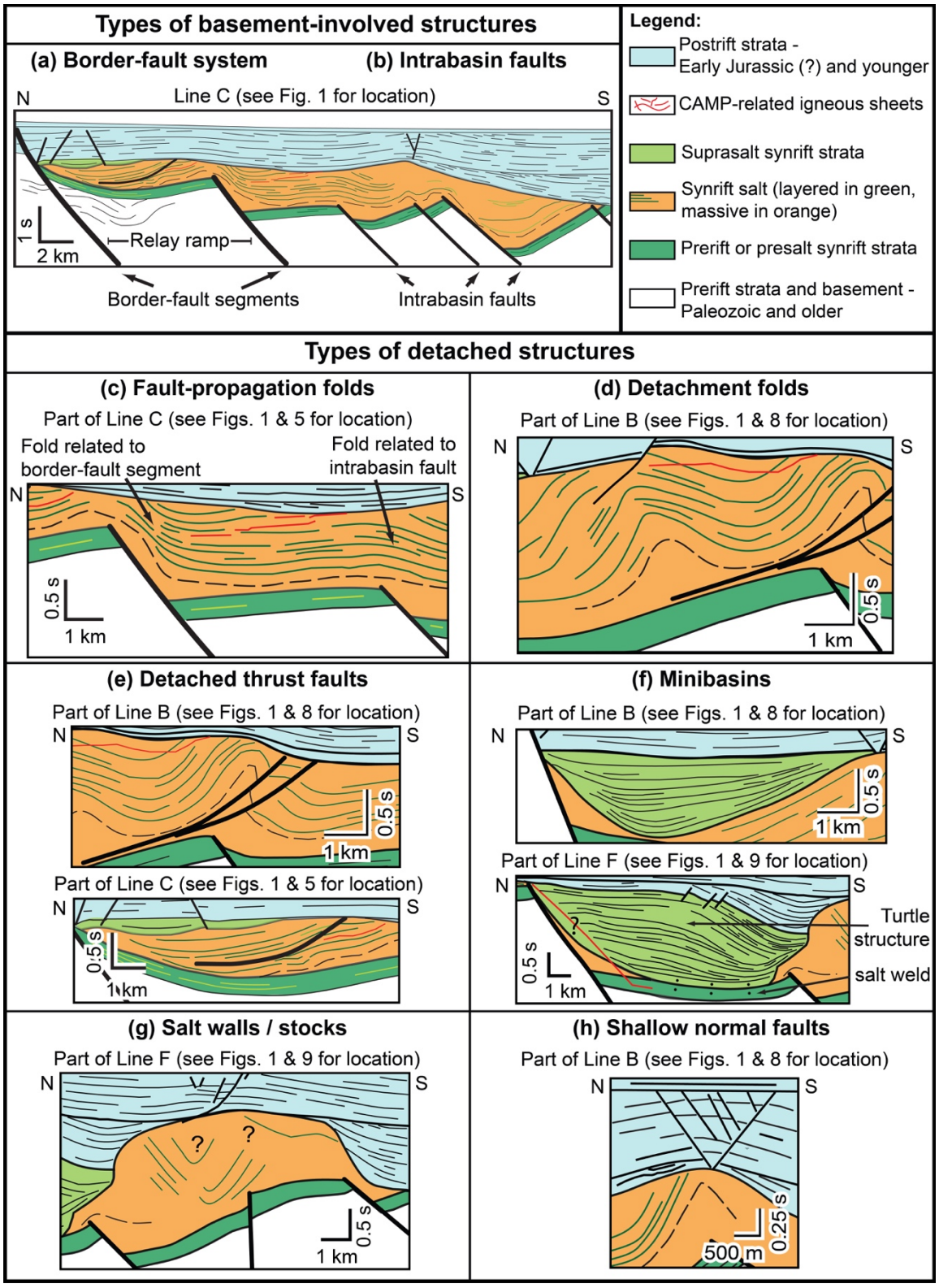

Figure 12. *Line drawings of seismic lines showing different types of structures in the study area. Basement-involved structures include: (a) segments of the border-fault system and (b) intrabasin*

faults. Detached structures include: (c) forced folds, (d) detachment folds, (e) detached thrust faults, (f) minibasins, (g) salt walls / stocks, and (h) shallow normal faults. Black dashed line indicates approximate boundary between lower massive salt and upper salt containing interbedded shales. Line drawings are displayed 1:1 assuming a velocity of 4.5 km/s.

Detachment folds also developed within the synrift package. For example, on Line B (Fig. 8), moderately to tightly folded synrift strata of Facies 3A overlie relatively undeformed fault blocks of Unit 1. This decoupling between the shallow and deep structures shows that the massive salt of Unit 2 acted as a major detachment level near the base of the synrift package. The detached anticlines and synclines are subparallel to the border-fault system (Fig. 13b). Low-angle faults (dip angle of < 30˚) with reverse separation offset the strata with Facies 3A (Fig. 8). These thrust faults are listric, dip toward the north, and commonly sole out within the massive salt of Unit 2. Other smaller faults with reverse separation are present within the synrift package, suggesting that multiple detachment surfaces exist within the interbedded shale and rock salt of Facies 3A (Fig. 7a). Based on a lack of growth beds, the detached folds and faults formed after the deposition of the affected synrift strata. The truncation of these folded and faulted strata by the breakup unconformity indicates that they formed before and/or during the formation of the unconformity.

Detached structures also include salt walls and stocks (composed of Units 2 and 3) that overlie relatively undeformed fault blocks of Unit 1 (Figs. 9, 12g) and have heights reaching up to 2.5 seconds TWTT (~ 5.6 km with a velocity of 4.5 km/s). In map view, salt stocks have diameters of ~ 5-10 km, whereas the salt walls are 5-to-10 km wide, more than 20-km long, and are parallel-to-subparallel to the strike of the border-fault segments (Fig. 13a).

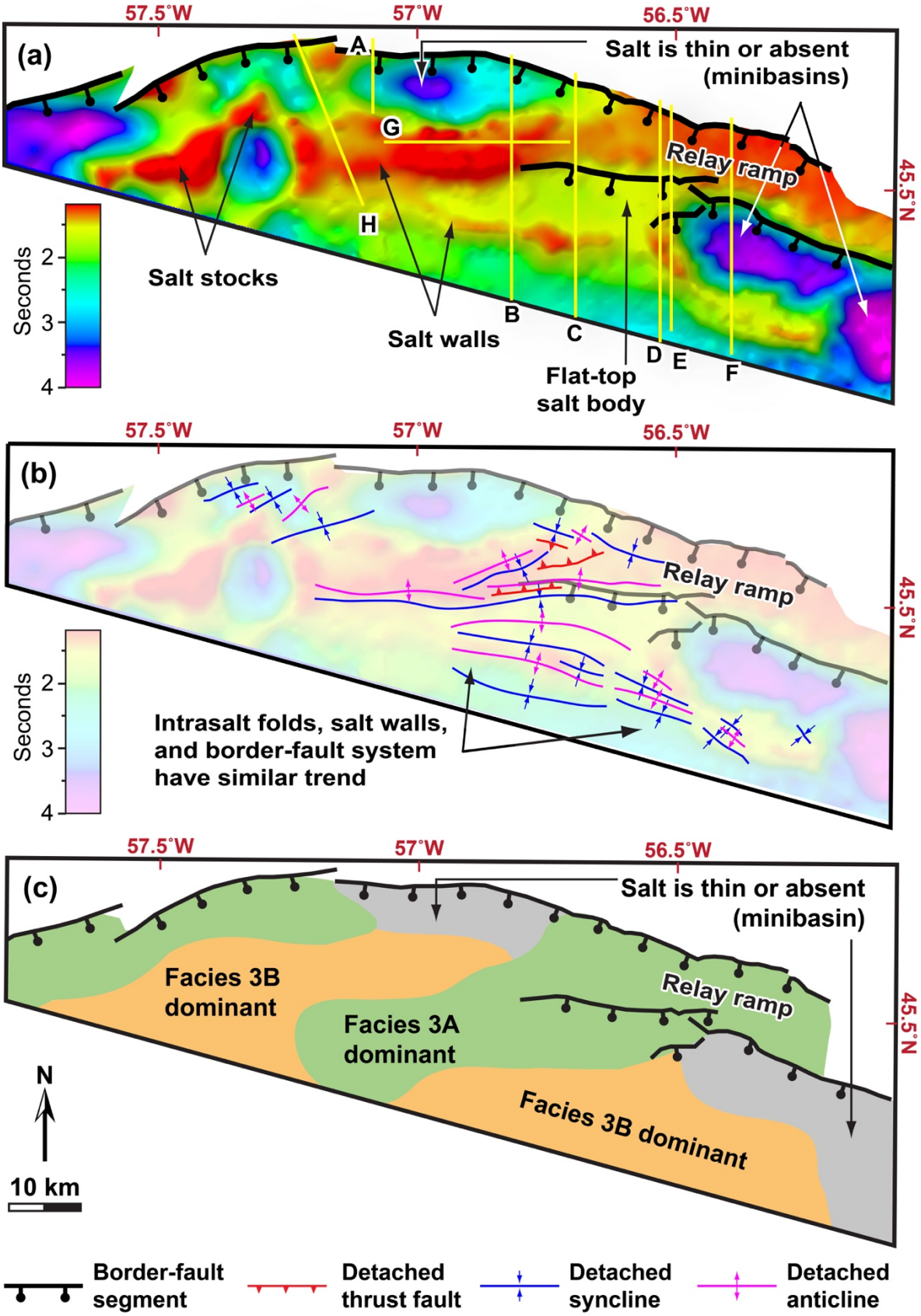
57.5°W
57°W
56.5°W
45.5°N
(a)
A
G
H
B
C
D
E
F
Salt is thin or absent
(minibasins)
Relay ramp
Salt stocks
Salt walls
Flat-top
salt body
Seconds
2
3
4
(b)
Relay ramp
Intrasalt folds, salt walls,
and border-fault system
have similar trend
(c)
Salt is thin or absent
(minibasin)
Facies 3B
dominant
Facies 3A
dominant
Relay ramp
Facies 3B dominant
N
10 km
Border-fault
segment
Detached
thrust fault
Detached
syncline
Detached
anticline

Figure 13. (a) *Time-structure map of top Argo salt,* ***(b)*** *map of interpreted intrasalt structures, and* ***(c)*** *map showing distribution of Facies 3A (consisting of interbedded salt and shale) and Facies 3B (consisting of mostly massive rock salt with limited interbedded shale). Facies 3A is dominant near the border-fault system and relay ramps. Gray areas denote regions with thin or absent salt related to evacuation caused by sediment loading (i.e., minibasin formation). Note that the two-way travel time for the top of the Argo salt is low above salt walls and stocks and near the elevated, eastern end of the relay ramp. Yellow lines in Figure 13a show the location of the seismic lines described in the text.*

Internal deformation within the walls and stocks includes tightly folded and faulted beds (Figs. 9, 13b). The surrounding synrift and postrift strata thicken and/or thin toward the walls and stocks (Figs. 9, 14). As mentioned previously, salt-withdrawal minibasins associated with Unit 4 developed adjacent to the salt walls and stocks (Figs. 9, 13a). Most minibasins developed directly to the south of the border-fault system, creating depocenters 20-to-30 km long and 10-to-15 km wide (Fig. 13a). Some minibasins directly overlie the presalt strata (Unit 1) and have primary salt welds at their base (Figs. 9, 12f). Many of these minibasins with a welded base are inverted and have turtle-structure anticlines with thicker strata near their axial surfaces (Figs. 9, 12f).

Shallow faults with normal separation are also present in the study area. These faults commonly offset the postrift strata and terminate at or offset the top of the synrift package (Figs. 8, 12h). Many of these faults formed as conjugate faults at the crest of anticlines that developed above the massive salt walls and stocks (Fig. 8). Most shallow faults with normal separation are planar. However, some faults that penetrate deeper into the synrift package are listric (Fig. 10).

None of these faults directly connects at depth with basement-involved faults except for a few faults that terminate against the border-fault segments in the north (Fig. 8). The timing of shallow faulting is poorly constrained because of the lack of associated growth beds. However, these faults offset the near-base Cretaceous unconformity (NBCU) and strata above it; thus, they likely developed in Cretaceous or later time (i.e., well after rifting).

4.6. CAMP-related igneous activity in the eastern Orpheus rift basin

The synrift package of the Orpheus rift basin contains anomalous, high-amplitude reflections with distinctive characteristics (Figs. 5, 7b). Many of these high-amplitude reflections terminate abruptly within the synrift section (Figs. 7b, 7d, 10). Although commonly parallel to subparallel to bedding, many locally cut through bedding, climbing to higher stratigraphic levels (Fig. 7b). Some high-amplitude reflections are present along basement-involved faults (Figs. 9, 10), whereas others bifurcate or splay, forming a complex array of high-amplitude reflections (Fig. 10). Although no well has drilled these high-amplitude reflections in the Orpheus rift basin, their distinctive seismic and geometric characteristics are indicative of intrusive igneous sheets (e.g., Planke et al., 2005). Igneous sheets, having high densities (2.8 - 3.0 g/cm^3) and seismic velocities (5.5 - 6.5 km/s) compared to those of sedimentary rocks (Planke et al., 1999; Berndt et al., 2000; Planke et al., 2005), produce high-amplitude reflections on seismic profiles. Thus, based on the distinctive characteristics of the high-amplitude reflections in the eastern Orpheus rift basin, we conclude that they are likely associated with intrusive igneous sheets.

The high-amplitude reflections are present throughout the synrift package in the eastern Orpheus rift basin. As discussed previously, synrift deposition in the region likely began by the Late Triassic and continued into the Early Jurassic (e.g., MacLean and Wade, 1992; Weston et

al., 2012; Withjack et al., 2012; Sues and Olsen, 2015). Thus, the magmatic activity associated with the high-amplitude reflections must have occurred after the deposition of the synrift strata preserved in the basin (i.e., during or/and after the Late Triassic). Furthermore, the breakup unconformity truncates some high-amplitude events (Figs. 7b, 14). Because the breakup unconformity separates the synrift strata from the overlying late Middle Jurassic postrift strata (OETR, 2014), magmatic activity must have occurred during and/or after the Late Triassic and during and/or before the late Middle Jurassic. Based on this time interval as well as the numerous

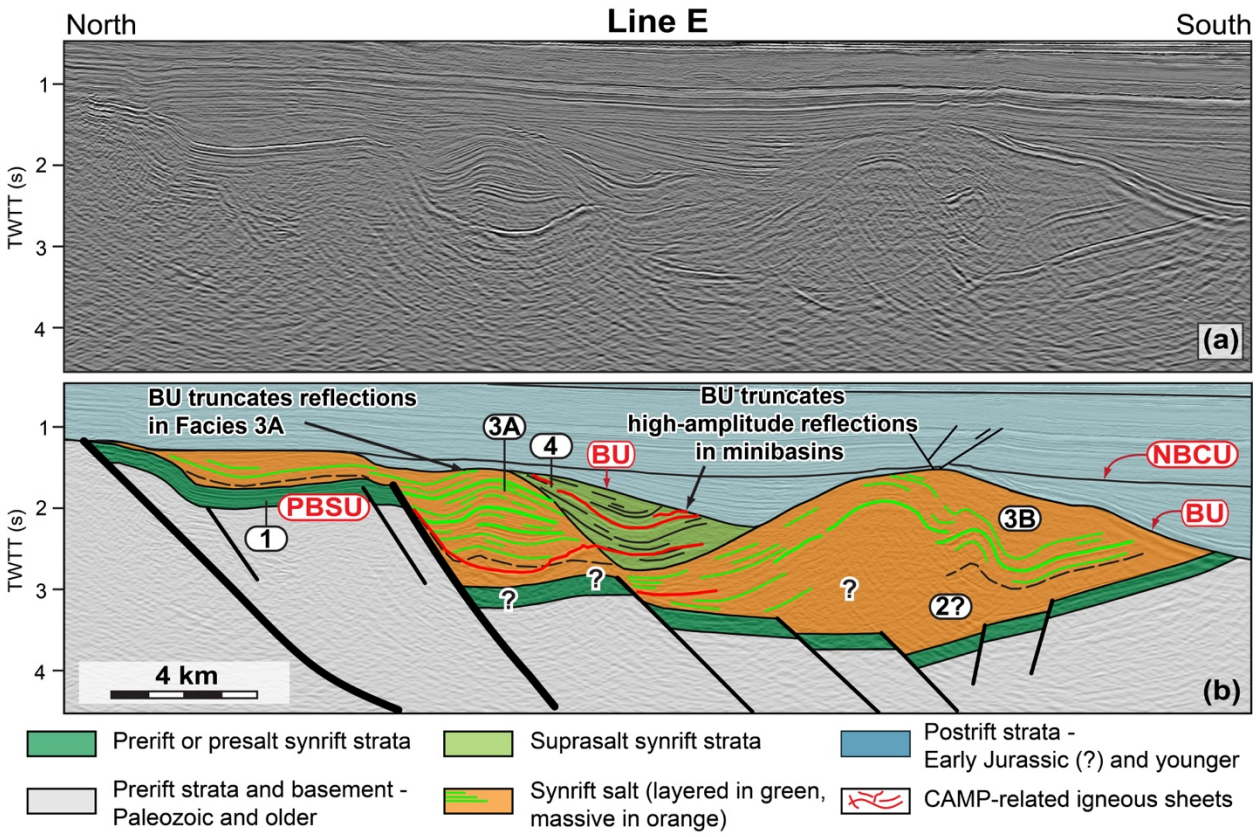

Figure 14. *Uninterpreted (a) and interpreted (b) versions of Line E (see Fig. 1b for location), showing truncation of high-amplitude reflections by breakup unconformity in minibasin. See caption of Figure 5 for description of Units 1-4. Dashed black line indicates approximate boundary between Units 2 and 3. PBSU: Prerift/base synrift unconformity; BU: Breakup unconformity; NBCU: Near-base Cretaceous unconformity; PBSU: Prerift/base synrift*

unconformity. CAMP: Central Atlantic Magmatic Province. TWTT: Two-way travel time. Seismic line is displayed 1:1 assuming a velocity of 4.5 km/s.

reports of CAMP-related igneous rocks in the region surrounding the Orpheus rift basin (e.g., Dostal and Greenough, 1992; McHone, 1992; Pe-Piper et al., 1992; Dostal and Durning, 1998; Cirilli et al., 2009; Jourdan et al., 2009), we propose that many of these igneous sheets are associated with CAMP, which as discussed previously, is a major igneous province that formed in latest Triassic to earliest Jurassic time (McHone, 1992; Pe-Piper et al., 1992; Olsen et al., 2003; Marzoli et al., 2011; Blackburn et al., 2013; Davies et al., 2017; Marzoli et al., 2018; Marzoli et al., 2019). It is possible that some igneous sheets, not truncated by the breakup unconformity, are associated with Early Cretaceous magmatic activity as, for example, reported by Zulfitriadi (2011).

5. AGE OF SYNRIFT UNITS AND TIMING OF DEFORMATION

5.1. Age of Units 1 to 4

We have concluded that the thick synrift package in the eastern Orpheus rift basin, with the exception of thin Eurydice Formation (?) at its base, is composed primarily of evaporitic sequences of the Argo Formation. Using well data from the western Orpheus rift basin, Bujak and Williams (1977), Barss et al. (1979), and MacRae and Rankin (2018) determined the palynological age of the Argo Formation as Early Jurassic (i.e., Hettangian-Sinemurian). Our work shows that, in the eastern Orpheus rift basin, igneous sheets likely related to CAMP intrude the entire synrift package and are truncated by the breakup unconformity. As mentioned previously, CAMP began during the latest Triassic and ended during the earliest Jurassic. Thus,

the deposition of the preserved synrift package in the eastern Orpheus rift basin would predate CAMP-related igneous activity, and the thick salt-rich section in the eastern Orpheus rift basin (Units 2 and 3) would have a Late Triassic age (Fig. 6). The salt-rich section in the eastern Orpheus rift basin would, thus, be equivalent to the salt of Late Triassic age encountered in the ENAM rift basins that surround the Orpheus rift basin, including the Mohican rift basin (Scotian Shelf) to the south (Weston et al., 2012; Deptuck and Kendell, 2017, 2020) and the Grand Banks rift basins to the north (Holser et al., 1988). It would be older than the salt of Early Jurassic age reported in the western Orpheus rift basin.

One possible explanation for the age difference for the synrift salt in the Orpheus rift basin is that salt deposition expanded to the west by the Early Jurassic, and erosion associated with the formation of the breakup unconformity (BU) subsequently removed synrift salt of Early Jurassic age from the study area. Another possible explanation is that subsidence and deposition ceased in the eastern Orpheus rift basin before the Early Jurassic but continued in the western Orpheus rift basin into the Early Jurassic. If the Argo Formation (i.e., Units 2 and 3) in the eastern Orpheus rift basin is Late Triassic in age, then underlying Unit 1, is Late Triassic or older. As mentioned previously, it is unclear whether this is part of the synrift Eurydice Formation or part of the prerift package (Fig. 6).

Despite limited information about the minibasins in the eastern Orpheus rift basin, we propose that sedimentary rocks of Unit 4 are likely synrift rocks of Late Triassic to earliest Jurassic age (Fig. 6). Unit 4 stratigraphically overlies the synrift salt of Unit 3 and is intruded by likely CAMP-related igneous sheets (Figs. 7d, 14), indicating that its deposition would have begun after the Late Triassic deposition of the salt of Unit 3 and before and/or during CAMP-related magmatic activity in the latest Triassic to earliest Jurassic. Minibasin formation ceased

before and/or during the development of the breakup unconformity. Identification of the breakup unconformity throughout the region (based on loop ties with areas where synrift and postrift strata are clearly distinguishable) indicates that the development of some minibasins resumed after the formation of the breakup unconformity (e.g., Figs. 9, 14). Although the age of the postrift strata in the minibasins is poorly constrained, they are older than the near-base Cretaceous unconformity (NBCU) and likely represent some of the oldest postrift rocks in the region (i.e., Middle Jurassic or older) (OETR, 2014).

5.2. Origin and timing of detached shortening

Detachment folds and detached thrust faults are common within the shale-rich salt facies of Unit 3 (i.e., Facies 3A). The lack of growth beds associated with these intrasalt structures and their truncation by the breakup unconformity indicates that most shortening occurred after the deposition of Unit 3 and before/during the formation of the breakup unconformity. The minibasins near the border-fault system contain synrift strata (Unit 4) that accumulated after the deposition of the synrift salt of Unit 3. The strata within the minibasins either thin or thicken toward and/or onlap onto salt bodies containing the intrasalt structures, indicating that minibasin formation and detached shortening were synchronous. Based on these observations, we propose that load-driven, lateral salt flow during the subsidence of the minibasins produced most of the shortening-related intrasalt structures. This is consistent with experimental studies that show that sediment loading above a salt layer (Ge et al., 1997a; Ge et al., 1997b; Hudec et al., 2009; Hudec and Jackson, 2011) can cause the salt to move laterally, leading to the formation of shortening-related intrasalt structures (Rowan et al., 2004).

The presence of CAMP-related igneous sheets is critical to constrain the timing of the detached intrasalt shortening. In our study area, likely CAMP-related igneous sheets cut across the folded and faulted strata of shale-rich synrift Unit 3 (Figs. 8, 10) and the synrift strata of Unit 4 within the minibasins (Figs. 7d, 14). Based on this observation, we propose that a significant amount of intrasalt shortening and coeval minibasin formation began before CAMP-related igneous activity. Specifically, because CAMP activity occurred at ~201 Ma (Marzoli et al., 2011; Blackburn et al., 2013; Davies et al., 2017; Marzoli et al., 2019), most intrasalt shortening began before the latest Triassic. Furthermore, because some minibasins contain both synrift and postrift strata (e.g., Figs. 9, 14), some intrasalt shortening and salt diapirism occurred after the formation of the breakup unconformity during the Early (?) to Late Jurassic.

The cause and timing of some shortening-related structures in the southernmost part of the basin, however, remain enigmatic. For example, some steeply dipping and folded strata of Facies 3A are present far south of the minibasins (e.g., Fig. 8), indicating that these structures may have an origin unrelated to minibasin formation. Because these folded strata are present above a major basement-involved, intrabasin fault and are truncated by the overlying breakup unconformity, the structures may have resulted from the reactivation of the fault with left-lateral and reverse components of slip during the rift-drift transition as proposed for faults in the adjacent and kinematically linked Fundy rift basin (Baum et al., 2008; Withjack et al., 2009; Withjack et al., 2010). Alternatively, analog modeling studies (e.g., Warsitzka et al., 2018) suggest that differential loading caused by sediment accumulation in the hanging walls of rift-related faults could produce salt inflation above the footwall of the faults. Either one or a combination of these scenarios is plausible to explain the formation of the folds in the southernmost part of the basin.

6. DISCUSSION

6.1. Factors that influence deformation style in salt-rich Orpheus rift basin

Structures vary considerably throughout the eastern Orpheus rift basin, ranging from basement-involved faults, to forced folds above basement-involved faults, to detachment folds and detached thrust faults, to intensely folded intrasalt stringers within massive salt walls and stocks (Figs. 12, 15). We propose that two factors profoundly impacted the deformational style of the eastern Orpheus rift basin and, by analogy, other salt-rich rift basins: 1) the basement-involved border-fault system, and 2) the mechanical stratigraphy of the synrift salt (i.e., massive vs. interbedded).

6.1.1. Arrangement and activity of basement-involved border-fault system

Rifting produced an E-striking border-fault system in the northern part of the eastern Orpheus rift basin. The shale-rich salt facies of Unit 3 (i.e., Facies 3A) is most prevalent in the northern part of the basin near the border-fault system and its relay ramps, whereas the shale-poor salt of Facies 3B developed farther from the border-fault system (Fig. 13c). This relationship suggests that the relay ramps of the border-fault system connected the footwall region outside of the basin with the hanging-wall basin interior, providing pathways for clastic sediments to enter the basin and promoting the deposition of interbedded salt and shale (Fig. 13c). Reports from other rift basins and modeling results suggest that ramp-parallel channel systems may deliver these clastic sediments into the hanging-wall region during rifting, allowing them to accumulate at the base of the relay ramps (Athmer et al., 2010; Athmer and Luthi, 2011; Hopkins and Dawers, 2018).

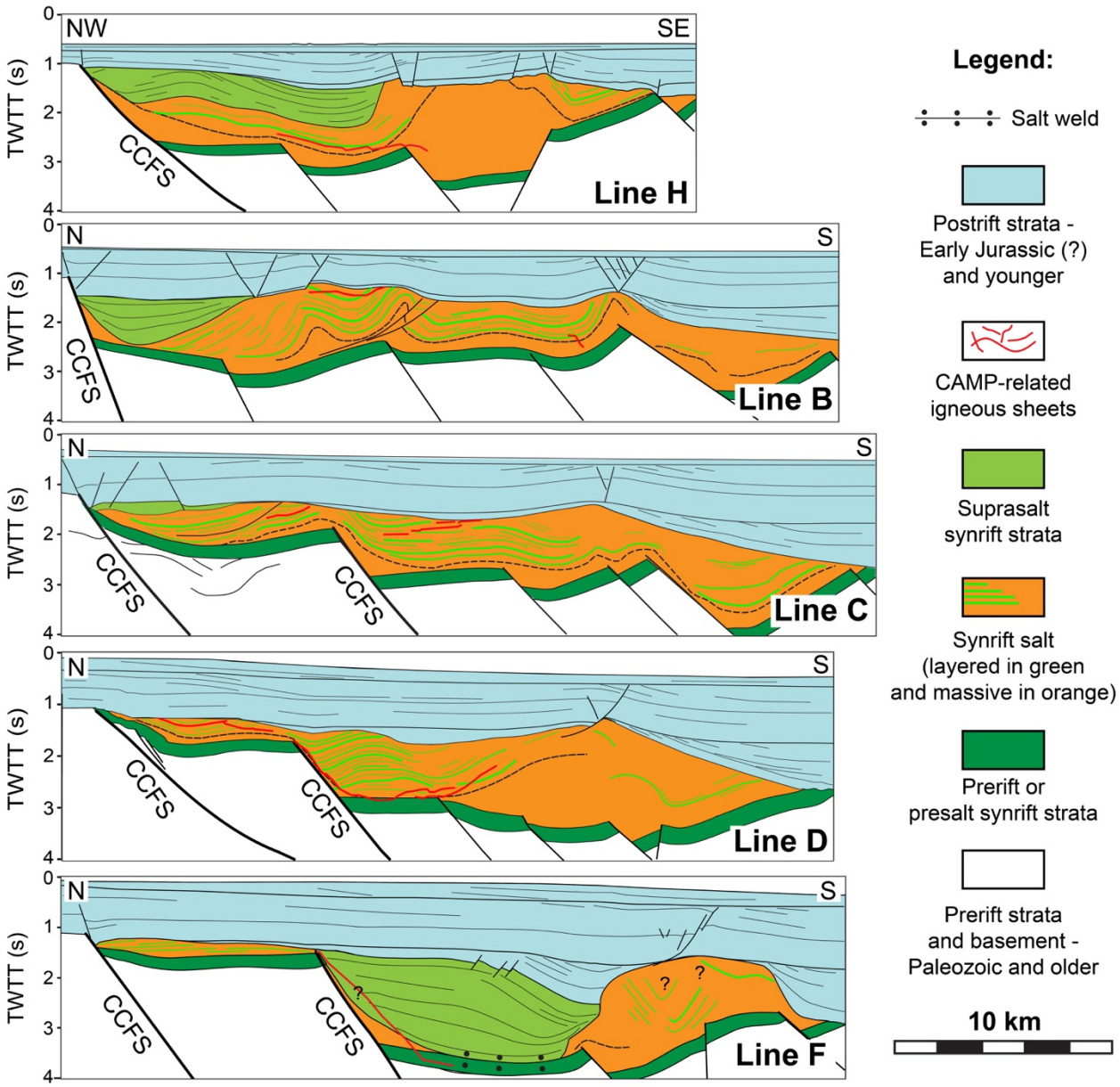

Figure 15. *Cross sections through eastern Orpheus rift basin based on 2D seismic-reflection data (see Figures 1b and 4 for locations). CCFS: Cobequid-Chedabucto fault system; CAMP: Central Atlantic Magmatic Province. Black dashed line in cross sections is approximate boundary between lower massive salt and upper layered salt. Seismic lines are displayed 1:1 assuming a velocity of 4.5 km/s.*

The sediments of the youngest synrift unit (Unit 4) accumulated within minibasins in the hanging wall directly adjacent to the border-fault system, suggesting an increased sediment influx into the basin from the adjacent footwall region during the later stages of rifting. The increased sediment influx likely reflects the development of footwall drainage systems that eroded the footwall rocks and delivered clastic sediments directly into the hanging walls of the border faults (Gawthorpe and Leeder, 2000; Densmore et al., 2004; Elliott et al., 2012). The deposition of these sedimentary rocks is important in producing a differential load above the salt (Hudec et al., 2009; Rowan, 2019), creating lateral salt flow toward the south, and triggering intrasalt shortening in the eastern Orpheus rift basin.

6.1.2. Mechanical stratigraphy of synrift salt

The presence of interbedded shales strongly influenced the bulk behavior of the synrift salt of the Argo Formation, which ultimately controlled the deformation style of the eastern Orpheus rift basin. Detachment folds and detached thrust faults deformed Facies 3A with its abundant interbedded shales and accommodated the shortening associated with lateral salt movement during minibasin formation (Fig. 12d-e). In contrast, Facies 3B with fewer interbedded shales exhibited a highly ductile behavior, combining with Unit 2 to form massive salt walls and stocks adjacent to the minibasins (Fig. 12g). These walls and stocks had complex internal deformation with tightly folded and faulted intrasalt stringers.

The contrasting behaviors of the massive salt in Unit 2 and the interbedded salt and shale in Facies 3A also promoted the formation of forced folds in the shallow synrift strata (Figs. 5, 7b). Specifically, the lower massive salt of Unit 2 with its highly ductile behavior decoupled the deep and shallow deformation. As a result, broad forced folds developed within Facies 3A to

accommodate the displacement on the underlying basement-involved faults. Our interpretation is consistent with the results of scaled experimental models that show the presence of salt can decouple the deep and shallow deformation and facilitate the formation of forced folds above a normal fault (Jackson and Vendeville, 1994; Withjack and Callaway, 2000).

6.2. The structural evolution of the eastern Orpheus basin during rifting

The E-striking, S-dipping border-fault system of the eastern Orpheus rift basin began to develop by the Late Triassic. Unit 2 (i.e., the massive salt of the lower Argo Formation) accumulated within a wide rift basin above Unit 1 (the synrift Eurydice Formation or a prerift unit) (Fig. 16a). As rifting continued, major relay ramps developed within the border-fault system, influencing depositional patterns of the upper Argo Formation (Unit 3) (Fig. 16b). The amount of interbedded shale within the upper Argo Formation varied laterally, depending on proximity to the relay ramps (Fig. 16b). Facies 3A with many interbedded shale layers formed within and near the relay ramps, whereas Facies 3B with few interbedded shale layers formed far from the relay ramps.

During the later stages of rifting (Late Triassic), deep-seated intrabasin faults formed south of the border-fault system (Fig. 16c). Many of these intrabasin faults dip to the south and offset Unit 1 with normal separation. Movement on these subsalt faults resulted in the development of broad monoclines (i.e., forced folds) within the overlying synrift strata. Additionally, minibasins developed adjacent to the border-fault system with deposition of alluvial fans and/or the accumulation of talus-slope deposits in the hanging wall. As the minibasins developed, sedimentary loading forced the underlying salt to move laterally toward the south, producing detachment folds, detached thrust faults, and salt walls and stocks (Fig. 16c). In latest

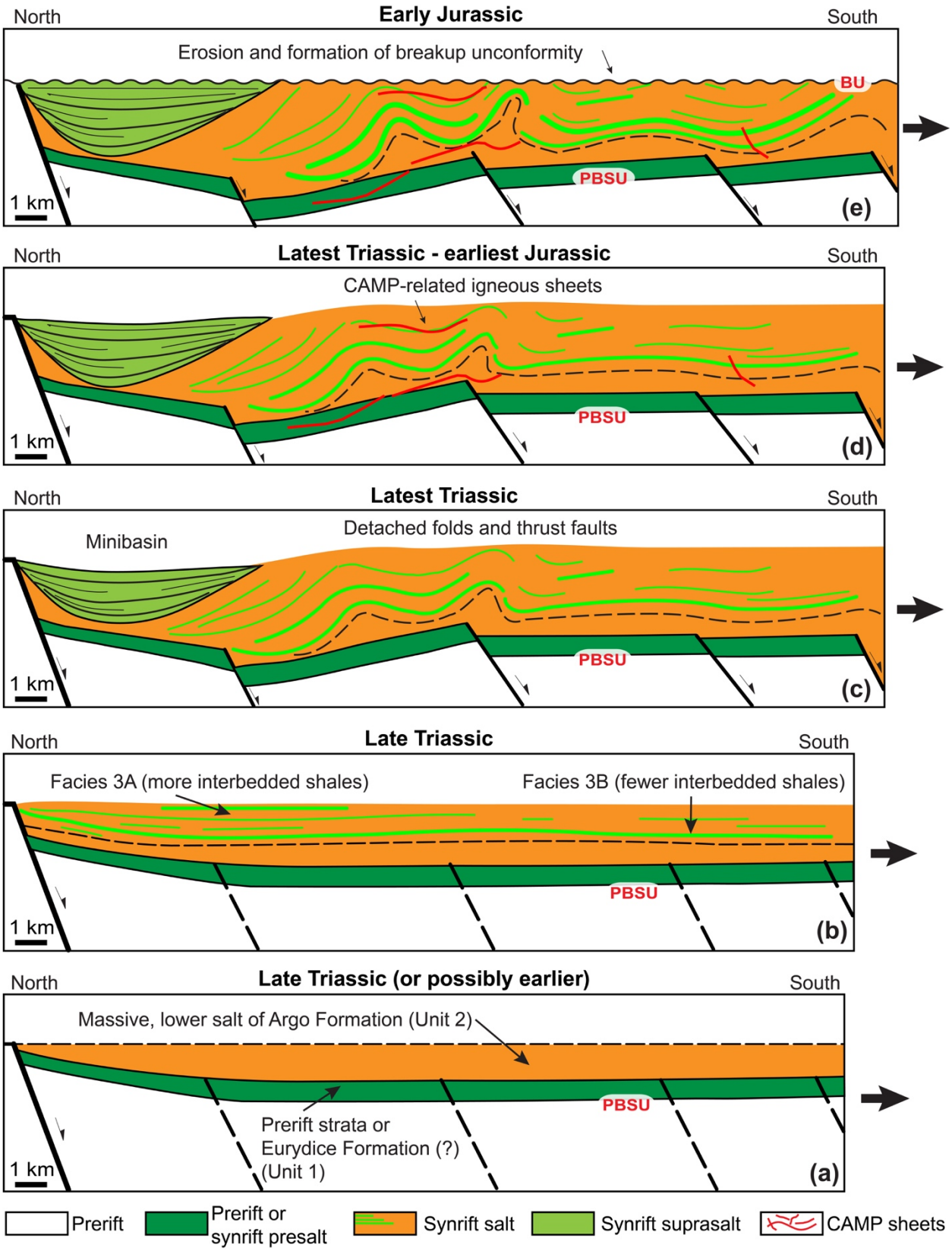
North
Early Jurassic
South
Erosion and formation of breakup unconformity
BU
PBSU
1 km
(e)
North
Latest Triassic - earliest Jurassic
South
CAMP-related igneous sheets
PBSU
1 km
(d)
North
Latest Triassic
South
Minibasin
Detached folds and thrust faults
PBSU
1 km
(c)
North
Late Triassic
South
Facies 3A (more interbedded shales)
Facies 3B (fewer interbedded shales)
PBSU
1 km
(b)
North
Late Triassic (or possibly earlier)
South
Massive, lower salt of Argo Formation (Unit 2)
PBSU
Prerift strata or
Eurydice Formation (?)
(Unit 1)
1 km
(a)
Prerift
Prerift or
synrift presalt
Synrift salt
Synrift suprasalt
CAMP sheets

Figure 16. *Schematic restoration of Line B (see Fig. 1b for location), showing eastern Orpheus basin development during Late Triassic (or possibly earlier) to Early Jurassic. (**a**) During early rifting, the deposition of clastic sediments (Eurydice Formation?) may have preceded the deposition of the massive salt of the Argo Formation (Unit 2). Basement-involved faulting was focused on the northern border-fault system, producing a wide basin with widespread deposition. (**b**) As rifting progressed, the development of relay ramps on the border-fault system promoted the input of clastic sediments into the basin. This resulted in lateral variability of the Argo salt with interbedded salt near the relay ramps (Facies 3A) and more massive salt far from the relay ramps (Facies 3B). (**c**) Activity continued on the border-fault system and basement-involved, intrabasin faults developed. Also, minibasins (likely associated with differential sediment loading near the border-fault system) caused salt to move laterally, producing detached shortening and massive salt walls and stocks. **(d)** CAMP-related igneous sheets intruded the synrift strata. **(e)** Erosion and formation of breakup unconformity. BU: Breakup unconformity; PBSU: Prerift/base synrift unconformity; CAMP: Central Atlantic Magmatic Province. Black dashed line indicates approximate boundary between lower massive salt and upper salt containing interbedded shales.*

Triassic/earliest Jurassic time, widespread igneous activity associated with the Central Atlantic Magmatic Province (CAMP) affected the eastern Orpheus rift basin (Fig. 16d) with numerous igneous sheets intruding the entire synrift section (Units 1-4). During the transition from rifting to drifting in the Early Jurassic, the formation of the breakup unconformity (BU) led to erosion of the synrift section in the eastern Orpheus rift basin (Fig. 16e).

7. CONCLUSIONS

1. The thick synrift package of the eastern Orpheus rift basin (locally more than 5 km) underlies a postrift package composed of Middle Jurassic and younger strata and overlies a prerift package of deformed Paleozoic strata and basement. The Cobequid-Chedabucto border-fault system, composed of offset fault segments and relay ramps, bounds the basin on the north. It strikes E-to-W, dips steeply to the south, and has normal separation that locally exceeds 5 km. Other structures in the basin include deep-seated intrabasin faults with normal separation, forced folds above the deep-seated faults, detachment folds and detached thrust faults, and salt walls and stocks.
2. The synrift package has several distinct units. Unit 1, with its deep stratigraphic location and relatively brittle behavior, may be part of the Eurydice Formation, the oldest synrift formation in the region composed of clastic sedimentary rocks. Alternatively, Unit 1, lacking clear rift-related growth geometries, may be part of the prerift package. Units 2 and 3 together likely represent synrift salt of the Argo Formation. Unit 2 is massive, whereas the overlying Unit 3 has two interfingering facies. Facies 3A is interpreted to consist of interbedded salt and shales (i.e., it is a layered evaporite sequence) and Facies 3B represents mostly massive salt with few interbedded shale layers. Unit 4, the youngest synrift unit, accumulated exclusively within minibasins near the border-fault system. The lithology of Unit 4 is unclear. Its proximity to the northern border-fault system, however, suggests that it might consist, at least in part, of coarse-grained and poorly sorted alluvial-fan or talus-slope deposits.
3. All of the synrift strata in the eastern Orpheus rift basin are intruded by igneous sheets likely associated with the Central Atlantic Magmatic Province (CAMP) that developed

during the latest Triassic to earliest Jurassic. If so, the synrift units in the eastern Orpheus rift basin are mostly Late Triassic in age, and the synrift salt in the eastern Orpheus rift basin is older than that encountered in wells from the western part of the basin, suggesting that: 1) salt deposition expanded to the west during the Early Jurassic, and erosion associated with the formation of the breakup unconformity subsequently removed the synrift salt of Early Jurassic age from the eastern Orpheus rift basin, or 2) subsidence and deposition ceased in the eastern Orpheus rift basin before the Early Jurassic but continued in the western Orpheus rift basin into the Early Jurassic.

4. The synrift and early postrift evolution of the eastern Orpheus rift basin was complex involving: 1) the development of the northern border-fault system and the formation of a wide rift basin during the early stages of rifting, 2) continued activity on the border-fault system, the development of intrabasin basement-involved faults, and the coeval development of minibasins, detached shortening-related structures, and salt diapirs, 3) the emplacement of CAMP-related igneous sheets, and 4) erosion and the formation of the breakup unconformity during the transition from rifting to drifting.
5. Two primary factors influenced the style of deformation in the eastern Orpheus rift basin during and after rifting: 1) the arrangement and activity of the basement-involved border faults, and 2) the mechanical stratigraphy of the synrift salt. Relay ramps of the border-fault system provided pathways for clastic sediments to enter the salt-rich rift basin. As a result, the sedimentation patterns of the synrift Argo Formation (i.e., Unit 3) varied basinward from interbedded salt and shales (Facies 3A) to predominantly rock salt (Facies 3B). Subsequent minibasin development near the border-fault system caused the underlying salt to flow laterally to the south, producing salt walls and/or stocks and

detached shortening-related structures. The proportion of salt-to-shale controlled the bulk deformational behavior of the synrift Argo Formation. The shale-rich Facies 3A of the Argo Formation accommodated the shortening associated with lateral salt flow during minibasin formation by developing detached folds and thrust faults. In contrast, the shale-poor Facies 3B of the Argo Formation had a highly ductile behavior, and, together with Unit 2, formed salt walls and stocks.

8. ACKNOWLEDGMENTS

We would like to thank our colleague, Zulfitriadi Syamsir, for his many valuable geologic and geophysical contributions and insights during this study. We thank TGS, ConocoPhillips, the Canadian Department of Natural resources, the Canada-Nova Scotia Offshore Petroleum Board (CNSOPB), and Suncor Energy for providing the 2D seismic-reflection data used in this study. We acknowledge the generosity of Schlumberger for providing Petrel, the software tool used to interpret the seismic data. We thank Husky Energy for providing general support for the Rutgers Structure Group and Iain Sinclair and Christopher Potter for their geologic insights. We also thank Rutgers University for providing support during this study. This paper was significantly improved by the reviews of Mark Rowan, Mark Deptuck, and Juan Soto. We also thank James Granath and Gabor Tari for handling manuscript and editorial input. Finally, we dedicate this paper to Bert Bally who was an inspiration to generations of geoscientists. He had incredible wisdom and insight, and, more importantly, he was a kind, generous person and a caring mentor.

9. REFERENCES

Ainsworth, N. R., Riley, L. A., Bailey, H. W., Coles, G. P., & Gueinn, K. J. (2016). Jurassic-Tertiary Stratigraphy of the Southern Newfoundland Margin - Wells: East Wolverine G-

37, Eider M-75, Emerillon M-75 & Narwhal F-99. *Riley Geoscience Limited. Report prepared for Nalcor Energy.*

Allen, P. A., & Heller, P. L. (2012). Dispersal and Preservation of Tectonically Generated Alluvial Gravels in Sedimentary Basins. In C. Busby & A. Azor (Eds.), *Tectonics of Sedimentary Basins* (pp. 111-130).

Ascoli, P. (1988). Mesozoic-Cenozoic foraminiferal, ostracod and calpionellid zonation of the North Atlantic margin of North America: Georges Bank-Scotian basins and northeastern Grand Banks (Jeanne d'Arc, Carson and Flemish Pass basins). Biostratigraphic correlation of 51 wells. *Geological Survey of Canada, Open File #1791*, 41.

Athmer, W., Groenenberg, R. M., Luthi, S. M., Donselaar, M. E., Sokoutis, D., & Willingshofer, E. (2010). Relay ramps as pathways for turbidity currents: a study combining analogue sandbox experiments and numerical flow simulations. *Sedimentology, 57*(3), 806-823. doi:10.1111/j.1365-3091.2009.01120.x

Athmer, W., & Luthi, S. M. (2011). The effect of relay ramps on sediment routes and deposition: A review. *Sedimentary Geology, 242*(1-4), 1-17. doi:10.1016/j.sedgeo.2011.10.002

Barss, M. S., Bujak, J. P., & Williams, G. L. (1979). Palynological zonation and correlation of sixty-seven wells, eastern Canada. *Geological Survey of Canada, Paper 78-24*.

Baum, M. S., Withjack, M. O., & Schlische, R. W. (2008). *The Ins and Outs of Buttress Folds: Examples from the Inverted Fundy Rift Basin, Nova Scotia and New Brunswick, Canada*. Paper presented at the Central Atlantic Conjugate Margins Conference, Halifax.

Berndt, C., Skogly, O. P., Planke, S., Eldholm, O., & Mjelde, R. (2000). High-velocity breakup-related sills in the Vøring Basin, off Norway. *Journal of Geophysical Research: Solid Earth, 105*(B12), 28443-28454. doi:10.1029/2000jb900217

Blackburn, T. J., Olsen, P. E., Bowring, S. A., McLean, N. M., Kent, D. V., Puffer, J., McHone, G., Rasbury, E. T., & Et-Touhami, M. (2013). Zircon U-Pb Geochronology Links the End-Triassic Extinction with the Central Atlantic Magmatic Province. *Science, 340*(6135), 941-945. doi:10.1126/science.1234204

Bowman, S. J., Pe-Piper, G., Piper, D. J. W., Fensome, R. A., & King, E. L. (2012). Early Cretaceous volcanism in the Scotian Basin. *Canadian Journal of Earth Sciences, 49*(12), 1523-1539. doi:10.1139/e2012-063

Bujak, J. P., & Williams, G. L. (1977). Jurassic palynostratigraphy of offshore eastern Canada. In F. M. Swain (Ed.), *Stratigraphic Micropaleontology of Atlantic Basin and Borderlands, Developments in Paleontology and Stratigraphy* (Vol. 6, pp. 321-339). Amsterdam: Elsevier.

Callot, J. P., Ribes, C., Kergaravat, C., Bonnel, C., Temiz, H., Poisson, A., Vrielynck, B., Salel, J. F., & Ringenbach, J. C. (2014). Salt tectonics in the Sivas basin (Turkey): crossing salt walls and minibasins. *Bulletin De La Societe Geologique De France, 185*(1), 33-42. doi:DOI 10.2113/gssgfbull.185.1.33

Cirilli, S., Marzoli, A., Tanner, L., Bertrand, H., Buratti, N., Jourdan, F., Bellieni, G., Kontak, D., & Renne, P. R. (2009). Latest Triassic onset of the Central Atlantic Magmatic Province (CAMP) volcanism in the Fundy Basin (Nova Scotia): New stratigraphic constraints. *Earth and Planetary Science Letters, 286*(3-4), 514-525. doi:10.1016/j.epsl.2009.07.021

Davies, J., Marzoli, A., Bertrand, H., Youbi, N., Ernesto, M., & Schaltegger, U. (2017). End-Triassic mass extinction started by intrusive CAMP activity. *Nat Commun, 8*, 15596. doi:10.1038/ncomms15596

Densmore, A. L., Dawers, N. H., Gupta, S., Guidon, R., & Goldin, T. (2004). Footwall topographic development during continental extension. *Journal of Geophysical Research-Earth Surface, 109*(F3). doi:10.1029/2003jf000115

Deptuck, M. E., & Altheim, B. (2018). Rift basins of the central LaHave Platform, offshore Nova Scotia. *CNSOPB Geoscience Open File Report, 2018-001MF*, 1-34.

Deptuck, M. E., & Kendell, K. L. (2017). A Review of Mesozoic-Cenozoic Salt Tectonics Along the Scotian Margin, Eastern Canada. In J. I. Soto, J. F. Flinch, & G. Tari (Eds.), *Permo-Triassic Salt Provinces of Europe, North Africa and the Atlantic Margins* (pp. 287-312).

Deptuck, M. E., & Kendell, K. L. (2020). Atlas of 3D seismic surfaces and thickness maps, central and southwestern Scotian Slope.

Diegel, F. A., Karlo, J. F., Schuster, D. C., Shoup, R. C., & Tauvers, P. R. (1995). Cenozoic structural evolution and tectono-stratigraphic framework of the northern Gulf coast continental margin. In M. P. A. Jackson, D. G. Roberts, & S. Snelson (Eds.), *Salt tectonics: a global perspective* (Vol. 65, pp. 109-1051): AAPG Memoir.

Dostal, J., & Durning, M. (1998). Geochemical constraints on the origin and evolution of early Mesozoic dikes in Atlantic Canada. *European Journal of Mineralogy, 10*, 79-93.

Dostal, J., & Greenough, J. D. (1992). Geochemistry and petrogenesis of the early Mesozoic North Mountain Basalts of Nova Scotia, Canada. In J. H. Puffer & P. C. Ragland (Eds.), *Eastern North American Mesozoic Magmatism* (Vol. 268): Geological Society of America, Special Paper.

Dunn, A. M., Reynolds, P. H., Clarke, D. B., & Ugidos, J. M. (1998). A comparison of the age and composition of the Shelburne dyke, Nova Scotia, and the Messejana dyke, Spain. *Canadian Journal of Earth Sciences, 35*(10), 1110-1115.

Elliott, G. M., Wilson, P., Jackson, C. A.-L., Gawthorpe, R. L., Michelsen, L., & Sharp, I. R. (2012). The linkage between fault throw and footwall scarp erosion patterns: An example from the Bremstein Fault Complex, offshore Mid-Norway. *Basin Research, 24*, 180-197. doi:10.1111/j.1365-2117.2011.00524.

Ford, M., Rohais, S., Williams, E. A., Bourlange, S., Jousselin, D., Backert, N., & Malartre, F. (2013). Tectono-sedimentary evolution of the western Corinth rift (Central Greece). *Basin Research, 25*(1), 3-25. doi:10.1111/j.1365-2117.2012.00550.x

Gawthorpe, R. L., Hurst, J. M., & Sladen, C. P. (1990). Evolution of Miocene footwall-derived coarse-grained deltas, Gulf of Suez, Egypt: Implications for Exploration. *AAPG Bulletin, 74*(7), 1077-1086.

Gawthorpe, R. L., & Leeder, M. R. (2000). Tecton-sedimentary evolution of active extensional basins. *Basin Research, 12*, 195-2018.

Ge, H., Jackson, M. P. A., Vendeville, B. C., Maier, M. O., & Handschy, J. W. (1997a). Deformation of Prograding Wedges over a Ductile Layer—Applications of Physical Models to Geologic Examples. *Gulf Coast Association of Geological Societies Transactions, XLVII*, 177-184.

Ge, H. X., Jackson, M. P. A., & Vendeville, B. C. (1997b). Kinematics and dynamics of salt tectonics driven by progradation. *AAPG Bulletin, 81*(3), 398-423.

Gibling, M. R., Culshaw, N., Rygel, M. C., & Pascucci, V. (2008). The Maritimes Basin of Atlantic Canada: Basin Creation and Destruction in the Collisional Zone of Pangea. In *Sedimentary Basins of the World* (Vol. 5, pp. 211-244).

Goteti, R., Ings, S. J., & Beaumont, C. (2012). Development of salt minibasins initiated by sedimentary topographic relief. *Earth and Planetary Science Letters, 339-340*, 103-116. doi:10.1016/j.epsl.2012.04.045

Gupta, S., Underhill, J. R., Sharp, I. R., & Gawthorpe, R. L. (1999). Role of fault interactions in controlling synrift sediment dispersal patterns: Miocene, Abu Alaqa Group, Suez Rift, Sinai, Egypt. *Basin Research, 11*(2), 167-189.

Hafid, M. (2000). Triassic-early Liassic extensional systems and their Tertiary inversion, Essaouira Basin (Morocco). *Marine and Petroleum Geology, 17*, 409 - 429.

Hafid, M., Zizi, M., Bally, A. W., & Ait Salem, A. (2006). Structural styles of the western onshore and offshore termination of the High Atlas, Morocco. *Comptes Rendus Geoscience, 338*(1-2), 50-64. doi:10.1016/j.crte.2005.10.007

Holser, W. T., Clement, G. P., Jansa, L. F., & Wade, J. A. (1988). Evaporite deposits of the North Atlantic rift. *Development in Geotectonics, 22*, 525-556.

Hopkins, M. C., & Dawers, N. H. (2018). The role of fault length, overlap and spacing in controlling extensional relay ramp fluvial system geometry. *Basin Research, 30*(1), 20-34. doi:10.1111/bre.12240

Hudec, M. R., & Jackson, M. P. A. (2011). *The salt mine: A digital atlas of salt tectonics*.

Hudec, M. R., Jackson, M. P. A., & Schultz-Ela, D. D. (2009). The paradox of minibasin subsidence into salt: Clues to the evolution of crustal basins. *Geological Society of America Bulletin, preprint*(2008). doi:10.1130/b26275.1

Jackson, C. A. L., Jackson, M. P. A., Hudec, M. R., & Rodriguez, C. R. (2015). Enigmatic structures within salt walls of the Santos Basin—Part 1: Geometry and kinematics from 3D seismic reflection and well data. *Journal of Structural Geology, 75*, 135-162. doi:10.1016/j.jsg.2015.01.010

Jackson, M. P. A., & Vendeville, B. C. (1994). Regional extension as a geologic trigger for diapirism. *Geological Society of America Bulletin, 106*(1), 57-73. doi:10.1130/0016-7606(1994)106<0057:Reaagt>2.3.Co;2

Jansa, L. F., Bujak, J. P., & Williams, G. L. (1980). Upper Triassic salt deposits of the western North Atlantic. *Canadian Journal of Earth Sciences, 17*(5), 547-559.

Jourdan, F., Marzoli, A., Bertrand, H., Cirilli, S., Tanner, L. H., Kontak, D. J., McHone, G., Renne, P. R., & Bellieni, G. (2009). 40Ar/39Ar ages of CAMP in North America: Implications for the Triassic–Jurassic boundary and the 40K decay constant bias. *Lithos, 110*(1-4), 167-180. doi:10.1016/j.lithos.2008.12.011

Kendell, K. L., Dehler, S., Deptuck, M., & Karim, A. (2012). Variations in salt expulsion style within the Sable Canopy Complex, central Scotian margin 1This article is one of a series of papers published in this CJES Special Issue on the theme of Mesozoic–Cenozoic geology of the Scotian Basin. *Canadian Journal of Earth Sciences, 49*(12), 1504-1522. doi:10.1139/e2012-069

Leeder, M. R., & Jackson, J. A. (1993). The interaction between normal faulting and drainage in active extensional basins, with examples from the western United States and central Greece. *Basin Research, 5*, 79-102.

MacLean, B. C., & Wade, J. A. (1992). Petroleum Geology of the Continental-Margin South of the Islands of St-Pierre and Miquelon, Offshore Eastern Canada. *Bulletin of Canadian Petroleum Geology, 40*(3), 222-253.

MacLean, B. C., & Wade, J. A. (1993). East Coast Basin Atlas Series: Seismic markers and stratigraphic picks in the Scotian Basin wells. *Geological Survey of Canada*, 276.

MacRae, R. A., & Rankin, S. K. (2018). *A palynological Triassic–Jurassic boundary section in the salt-bearing Argo F-38 well, Orpheus Graben, offshore Nova Scotia, Canada*. Paper presented at the Conjugate Margins Conference.

Manspeizer, W. (1988). A Stratigraphic Record from Morocco and North-America of Rifting, Drifting and Tethyan Transgressions of the Central Proto-Atlantic. *Journal of African Earth Sciences, 7*(2), 369-373. doi:Doi 10.1016/0899-5362(88)90081-4

Manspeizer, W., & Cousminer, H. L. (1988). Late Triassic-Early Jurassic synrift basins of the U.S. Atlantic margin. In R. E. Sheridan & J. A. Grow (Eds.), *The Geology of North America, The Atlantic Continental Margin* (Vol. I-2, pp. 197-216): Geological Society of America.

Martin-Martin, J. D., Verges, J., Saura, E., Moragas, M., Messager, G., Baques, V., Razin, P., Grelaud, C., Malaval, M., Joussiaume, R., Casciello, E., Cruz-Orosa, I., & Hunt, D. W. (2017). Diapiric growth within an Early Jurassic rift basin: The Tazoult salt wall (central High Atlas, Morocco). *Tectonics, 36*(1), 2-32. doi:10.1002/2016tc004300

Marzoli, A., Bertrand, H., Youbi, N., Callegaro, S., Merle, R., Reisberg, L., Chiaradia, M., Brownlee, S. I., Jourdan, F., Zanetti, A., Davies, J. H. F. L., Cuppone, T., Mahmoudi, A., Medina, F., Renne, P. R., Bellieni, G., Crivellari, S., El Hachimi, H., Bensalah, M. K., Meyzen, C. M., & Tegner, C. (2019). The Central Atlantic Magmatic Province (CAMP) in Morocco. *Journal of Petrology, 60*(5), 945-996. doi:10.1093/petrology/egz021

Marzoli, A., Callegaro, S., Dal Corso, J., Davies, J. H. F. L., Chiaradia, M., Youbi, N., Bertrand, H., Reisberg, L., Merle, R., & Jourdan, F. (2018). The Central Atlantic Magmatic Province (CAMP): A Review. In *The Late Triassic World* (pp. 91-125).

Marzoli, A., Jourdan, F., Puffer, J. H., Cuppone, T., Tanner, L. H., Weems, R. E., Bertrand, H., Cirilli, S., Bellieni, G., & De Min, A. (2011). Timing and duration of the Central Atlantic magmatic province in the Newark and Culpeper basins, eastern U.S.A. *Lithos, 122*(3-4), 175-188. doi:10.1016/j.lithos.2010.12.013

McHone, J. G. (1992). Mafic dike suites within Mesozoic igneous provinces of New England and Atlantic Canada. *Geological Society of America Special Paper, 268*.

Medina, F. (1995). Syn- and postrift evolution of the El Jadida - Agadir basin (Morocco): constraints for the rifting model of the central Atlantic. *Canadian Journal of Earth Sciences, 32*, 1273 - 1291.

OETR. (2014). *Offshore Energy Technical Research Association. Play Fairway Analysis - Laurentian Basin, Canada. Nova Scotia Department of Energy.* Retrieved from https://energy.novascotia.ca/oil-and-gas/offshore/play-fairway-analysis/analysis/laurentian-sub-basin

Olsen, P. E. (1997). Stratigraphic record of the early Mesozoic breakup of Pangea in the Laurasia-Gondwana rift system. *Annual Review of Earth and Planetary Sciences, 25*, 337-401. doi:10.1146/annurev.earth.25.1.337

Olsen, P. E., & Et-Touhami, M. (Eds.). (2008). *Field trip 1: Tropic to subtropical syntectonic sedimentation in the Permian to Jurassic Fundy rift basin, Atlantic Canada, in relation to the Moroccan conjugate margin*. Halifax, N. S., Canada: Dalhousie University.

Olsen, P. E., Kent, D. V., Cornet, B., Witte, W. K., & Schlische, R. W. (1996). High-resolution stratigraphy of the Newark rift basin (early Mesozoic, eastern North America). *Geological Society of America Bulletin, 108*(1), 40-77. doi:10.1130/0016-7606(1996)108<0040:Hrsotn>2.3.Co;2

Olsen, P. E., Kent, D. V., Et-Touhami, M., & Puffer, J. (2003). Cyclo-, magneto-, and bio-stratigraphic constraints on the duration of the CAMP event and its relationship to the Triassic-Jurassic boundary. *Geophysical Monograph, 136*, 7-32.

Olsen, P. E., & Schlische, R. W. (1990). Transtensional Arm of the Early Mesozoic Fundy Rift Basin - Penecontemporaneous Faulting and Sedimentation. *Geology, 18*(8), 695-698. doi:Doi 10.1130/0091-7613(1990)018<0695:Taotem>2.3.Co;2

Pascucci, V., Gibiling, M. R., & Willamson, M. A. (1999). Seismic stratigraphy analysis of Carboniferous strata on the Burin Platform offshore eastern Canada. *Bulletin of Canadian Petroleum Geology, 47*(3), 298-316.

Pe-Piper, G., Jansa, L. F., & Lambert, R. (1992). Early Mesozoic magmatism on the eastern Canadian margin: petrogenetic and tectonic significance. In J. H. Puffer & P. C. Ragland (Eds.), *Eastern North American Mesozoic Magmatism* (Vol. 268, pp. 13-36): GSA Special Papers.

Pe-Piper, G., & Piper, D. J. W. (2004). The effects of strike-slip motion along the Cobequid - Chedabucto - southwest Grand Banks fault system on the Cretaceous-Tertiary evolution of Atlantic Canada. *Canadian Journal of Earth Sciences, 41*(7), 799-808. doi:10.1139/e04-022

Peacock, D. C. P., & Sanderson, D. J. (1991). Displacements, segment linkage and relay ramps in normal fault zone. *Journal of Structural Geology, 16*(6), 721-733.

Planke, S., Alvestad, E., & Eldholm, O. (1999). Seismic characteristics of basaltic extrusive and intrusive rocks. *The Leading Edge, 18*(3), 342-348. doi:10.1190/1.1438289

Planke, S., Rasmussen, T., Rey, S. S., & Myklebust, R. (2005). *Seismic characteristics and distribution of volcanic intrusions and hydrothermal vent complexes in the Vøring and Møre basins.* Paper presented at the Geological Society, London, Petroleum Geology Conference series.

Rowan, M. G. (2019). Conundrums in loading-driven salt movement. *Journal of Structural Geology, 125*, 256-261. doi:10.1016/j.jsg.2018.04.010

Rowan, M. G., Peel, F. J., & Vendeville, B. C. (2004). Gravity-driven Fold Belts on Passive Margins. In K. R. McClay (Ed.), *Thrust tectonics and hydrocarbon systems* (pp. 157-182).

Rowan, M. G., Urai, J. L., Fiduk, J. C., & Kukla, P. A. (2019). Deformation of intrasalt competent layers in different modes of salt tectonics. *Solid Earth, 10*(3), 987-1013. doi:10.5194/se-10-987-2019

Saura, E., Verges, J., Martin-Martin, J. D., Mesager, G., Moragas, M., Razin, P., Grelaud, C., Joussiaume, R., Malaval, M., Homke, S., & Hunt, D. W. (2014). Syn- to post-rift diapirism and minibasins of the Central High Atlas (Morocco): the changing face of a mountain belt. *Journal of the Geological Society, 171*(1), 97-105. doi:10.1144/jgs2013-079

Schlische, R. W., Withjack, M. O., & Eisenstadt, G. (2002). An experimental study of the secondary deformation produced by oblique-slip normal faulting. *AAPG Bulletin, 86*(5), 885-906.

Schlische, R. W., Withjack, M. O., & Olsen, P. E. (2003). Relative Timing of CAMP, Rifting, Continental Breakup, and Basin Inversion: Tectonic Significance. In W. E. Hames, J. G. McHone, P. R. Renne, & C. Ruppel (Eds.), *The Central Atlantic Magmatic Province, Insights from Fragments of Pangea* (Vol. 136, pp. 33-59): American Geophysical Union, Geophysical Monograph.

Sinclair, I. K. (1993). Tectonism: the dominant factor in mid-Cretaceous deposition in the Jeanne d'Arc Basin, Grand Banks. *Marine and Petroleum Geology, 10*, 530-549.
Sinclair, I. K. (1995). Transpressional inversion due to episodic rotation of extensional stresses in Jeanne d'Arc Basin, offshore Newfoundland. In J. G. Buchanan & P. G. Buchanan (Eds.), *Basin Inversion* (Vol. 88, pp. 249-271): Geological Society, Special Publication.
Sinclair, I. K., Evans, J. E., Albrechtsons, E. A., & Sydora, L. J. (1999). The Hibernia Oilfield - effects of episodic tectonism on structural character and reservoir compartmentalization. *Petroleum Geology of Northwest Europe: Proceedings of the 5th Conference*, 517-528.
Sues, H.-D., & Olsen, P. E. (2015). Stratigraphic and temporal context and faunal diversity of Permian-Jurassic continental tetrapod assemblages from the Fundy rift basin, eastern Canada. *Atlantic Geology, 51*(1). doi:10.4138/atlgeol.2015.006
Tankard, A. J., Welsink, H. J., & Jenkins, W. A. M. (1989). Structural styles and stratigraphy of the Jeanne d'Arc Basin, Grand Banks of Newfoundland. In A. J. Tankard & H. R. Balkwill (Eds.), *Extensional tectonics and stratigraphy of the North Atlantic margins: AAPG Memoir* (Vol. 46, pp. 265-282): AAPG Memoir.
Tanner, L. H., & Brown, D. E. (1999). The Upper Triassic Chedabucto Formation: Guysborough County, Nova Scotia: depositional and tectonic context. *Atlantic Geology, 35*, 129-138.
Tanner, L. H., & Brown, D. E. (2003). *Tectonostratigraphy of the Orpheus graben, Scotian basin, offshore eastern Canada, and its relationship to the Fundy rift basin* (Vol. 2): Columbia University Press.
Tanner, L. H., & Hubert, J. F. (1991). Basalt breccias and conglomerates in the lower Jurassic McCoy Brook Formation, Fundy basin, Nova Scotia: Differentiation of talus and debris-flow deposits. *Journal of Sedimentary Petrology, 61*, 15-27.
Tari, G., & Jabour, H. (2013). Salt tectonics along the Atlantic margin of Morocco. In W. U. Mohriak, A. Danforth, P. J. Post, D. E. Brown, G. C. Tari, M. Nemcok, & S. T. Sinha (Eds.), *Conjugate Divergent Margins* (Vol. 369, pp. 337-353): Geological Society, London, Special Publications.
Teixell, A., Barnolas, A., Rosales, I., & Arboleya, M.-L. (2017). Structural and facies architecture of a diapir-related carbonate minibasin (lower and middle Jurassic, High Atlas, Morocco). *Marine and Petroleum Geology, 81*, 334-360. doi:10.1016/j.marpetgeo.2017.01.003
Van Gent, H., Urai, J. L., & de Keijzer, M. (2011). The internal geometry of salt structures – A first look using 3D seismic data from the Zechstein of the Netherlands. *Journal of Structural Geology, 33*(3), 292-311. doi:10.1016/j.jsg.2010.07.005
Verati, C., Rapaille, C., Féraud, G., Marzoli, A., Bertrand, H., & Youbi, N. (2007). 40Ar/39Ar ages and duration of the Central Atlantic Magmatic Province volcanism in Morocco and Portugal and its relation to the Triassic–Jurassic boundary. *Palaeogeography, Palaeoclimatology, Palaeoecology, 244*(1-4), 308-325. doi:10.1016/j.palaeo.2006.06.033
Wade, J. A., & MacLean, B. C. (1990). The geology of of the southeastern margin of Canada. In M. J. Keen & G. L. Williams (Eds.), *Geology of the continental margin of eastern Canada* (pp. 167 - 238): Geological Survey of Canada, Geology of Canada.
Wade, J. A., MacLean, B. C., & Williams, G. L. (1995). Mesozoic and Cenozoic Stratigraphy, Eastern Scotian Shelf - New Interpretations. *Canadian Journal of Earth Sciences, 32*(9), 1462-1473. doi:10.1139/e95-118
Warsitzka, M., Kukowski, N., & Kley, J. (2018). Salt flow direction and velocity during subsalt normal faulting and syn-kinematic sedimentation—implications from analytical

calculations. *Geophysical Journal International, 213*(1), 115-134. doi:10.1093/gji/ggx552

Welsink, H., & Tankard, A. (2012). Extensional tectonics and stratigraphy of the Mesozoic Jeanne d'Arc basin, Grand Banks of Newfoundland. In A. W. Bally & D. G. Roberts (Eds.), *Regional Geology and Tectonics: Phanerozoic Rift Systems and Sedimentary Basins* (pp. 373-381). Amsterdam: Elsevier.

Weston, J. F., MacRae, R. A., Ascoli, P., Cooper, M. K. E., Fensome, R. A., Shaw, D., & Williams, G. L. (2012). A revised biostratigraphic and well-log sequence-stratigraphic framework for the Scotian Margin, offshore eastern Canada. *Canadian Journal of Earth Sciences, 49*(12), 1417-1462. doi:10.1139/e2012-070

White, C. E., Kontak, D. J., DeMont, G. J., & Archibald, D. (2017). Remnants of Early Mesozoic basalt of the Central Atlantic Magmatic Province in Cape Breton Island, Nova Scotia, Canada. *Canadian Journal of Earth Sciences, 54*(4), 345-358. doi:10.1139/cjes-2016-0181

Willis, M. E., Lu, R. R., Campman, X., Toksoz, M. N., Zhang, Y., & de Hoop, M. V. (2006). A novel application of time-reversed acoustics: Salt-dome flank imaging using walkaway VSP surveys. *Geophysics, 71*(2), A7-A11. doi:10.1190/1.2187711

Withjack, M., Malinconico, M., & Durcanin, M. (2020). The "Passive" Margin of Eastern North America: Rifting and the Influence of Prerift Orogenic Activity on Postrift Development. *Lithosphere, 2020*(1). doi:10.2113/2020/8876280

Withjack, M. O., Baum, M. S., & Schlische, R. W. (2010). Influence of preexisting fault fabric on inversion-related deformation: A case study of the inverted Fundy rift basin, southeastern Canada. *Tectonics, 29*(6), n/a-n/a. doi:10.1029/2010tc002744

Withjack, M. O., & Callaway, S. (2000). Active normal faulting beneath a salt layer: An experimental study of deformation patterns in the cover sequence. *AAPG Bulletin, 84*(5), 627-651.

Withjack, M. O., & Schlische, R. W. (2005). *A Review of Tectonic Events on the Passive Margin of Eastern North America*. Paper presented at the 25th Annual Bob F. Perkins Research Conference, Houston, Texas.

Withjack, M. O., Schlische, R. W., & Baum, M. S. (2009). Extensional development of the Fundy rift basin, southeastern Canada. *Geological Journal, 44*(6), 631-651. doi:10.1002/gj.1186

Withjack, M. O., Schlische, R. W., Malinconico, M. L., & Olsen, P. E. (2013). Rift-basin development: Lessons from the Triassic–Jurassic Newark Basin of eastern North America. In W. U. Mohriak, A. Danforth, P. J. Post, D. E. Brown, G. C. tari, M. Nemcok, & S. T. Sinha (Eds.), *Conjugate Divergent Margins* (Vol. 369, pp. 301-321): Geological Society, London, Special Publications.

Withjack, M. O., Schlische, R. W., & Olsen, P. E. (1998). Diachronous rifting, drifting, and inversion on the passive margin of central eastern North America: An analog for other passive margins. *AAPG Bulletin, 82*(5), 817-835.

Withjack, M. O., Schlische, R. W., & Olsen, P. E. (2002). Rift-basin structure and its influence on sedimentary systems. In R. W. Renaut & G. M. Ashley (Eds.), *Sedimentation in Continental Rifts* (Vol. 73, pp. 57-81): SEPM Special Publication.

Withjack, M. O., Schlische, R. W., & Olsen, P. E. (2012). Development of the passive margin of Eastern North America: Mesozoic rifting, igneous activity, and breakup. In D. G. Roberts

& A. W. Bally (Eds.), *Regional Geology and Tectonics: Phanerozoic Rift Systems and Sedimentary Basins* (pp. 300-335): Elsevier.
Yilmaz, O. (1987). *Seismic Data Processing*. Tulsa, Oklahoma: Society of Exploration Geophysicists.
Zong, J. J., Stewart, R. R., Dyaur, N., & Myers, M. T. (2017). Elastic properties of rock salt: Laboratory measurements and Gulf of Mexico well-log analysis. *Geophysics, 82*(5), D303-D317. doi:10.1190/Geo2016-0527.1
Zulfitriadi. (2011). *The Mesozoic Orpheus rift basin, offshore Nova Scotia and Newfoundland, Canada: Synrift and early postrift evolution of a well-imaged North Atlantic rift basin.* (Masters). Rutgers University, New Brunswick.